CHARACTERIZATION OF INERTIAL AND PRESSURE EFFECTS IN HOMOGENEOUS TURBULENCE

A Thesis

by

RAVI KIRAN BIKKANI

Submitted to the Office of Graduate Studies of
Texas A&M University
in partial fulfillment of the requirements for the degree of

MASTER OF SCIENCE

August 2005

Major Subject: Aerospace Engineering

CHARACTERIZATION OF INERTIAL AND PRESSURE EFFECTS IN HOMOGENEOUS TURBULENCE

A Thesis

by

RAVI KIRAN BIKKANI

Submitted to the Office of Graduate Studies of
Texas A&M University
in partial fulfillment of the requirements for the degree of

MASTER OF SCIENCE

Approved by:

Chair of Committee,	Sharath S. Girimaji
Committee Members,	Rodney D. Bowersox
	Prabir Daripa
Head of Department	Helen L. Reed

August 2005

Major Subject: Aerospace Engineering

ABSTRACT

Characterization of Inertial and Pressure Effects in Homogeneous Turbulence.

(August 2005)

Ravi Kiran Bikkani, B.Tech., Indian Institute of Technology Madras

Chair of Advisory Committee: Dr. Sharath S. Girimaji

The objective of the thesis is to characterize the linear and nonlinear aspects of inertial and pressure effects in turbulent flows. In the first part of the study, computations of Navier-Stokes and 3D Burgers equations are performed in the rapid distortion (RD) limit to analyze the inviscid linear processes in homogeneous turbulence. By contrasting the results of Navier- Stokes RD equations and Burgers RD equations, the effect of pressure can be isolated. The evolution of turbulent kinetic energy and anisotropy components and invariants are examined. In the second part of the thesis, the velocity gradient dynamics in turbulent flows are studied with the help of inviscid 3D Burgers equations and restricted Euler equations. The analytical asymptotic solutions of velocity gradient tensor are obtained for both Burgers and restricted Euler equations. Numerical computations are also performed to identify the stable solutions. The results are compared and contrasted to identify the effect of pressure on nonlinear velocity gradient dynamics. Of particular interest are the sign of the intermediate principle strain-rate and tendency of vorticity to align with the intermediate principle strain-rate. These aspects of velocity gradients provide valuable insight into the role of pressure in the energy cascade process.

To mom and dad

ACKNOWLEDGMENTS

I would like to express my gratitude to all those wonderful people that have helped me in various different ways over the past couple of years. First and foremost I would like to thank my research advisor Dr. Girimaji for his continuous support, advice and guidance during various stages of my Masters program. I would like to thank Dr. Karpetis and Dr. Daripa for reviewing my thesis and providing valuable feedback. The courses that I took with Dr. Daripa were of immense help for my research work.

I greatly appreciate the help that I received from Aditya, Josh, Huidan, Sunil and all the other members of the Turbulence research group. I would like to thank Ravi, Navendu, Rohit and Manpreet for being such wonderful roommates making my stay here in College Station a memorable experience. My thanks are also due to Ms. Karen Knabe and Ms. Donna Holick for their assistance with the various administrative issues.

TABLE OF CONTENTS

CHAPTER Page

LIST OF FIGURES

FIGURE Page

CHAPTER I

INTRODUCTION

The thesis is divided into two parts, each addressing different aspects of homogeneous turbulence. In the first part, we use 'Rapid Distortion Theory' to study the linear aspects of inertial and pressure effects in turbulence physics. In the second part of the thesis, we examine the effect of inertial and pressure terms on the nonlinear velocity gradient dynamics of homogeneous turbulent flows using Burgers equation and restricted Euler equation.

1.1 Rapid distortion theory

Rapid distortion theory (RDT) is an important tool for investigating turbulence physics. In the rapid distortion limit, the mean flow timescale is much smaller than that of the fluctuating flow so that the nonlinear interactions among fluctuating modes can be neglected. In this limit, the evolution equations are linear in fluctuating velocity. In inviscid homogeneous RDT, the non-linear effects such as cascading (non-linear inertial), turbulent transport (absent in homogeneous turbulence) and dissipation (non-linear viscous) are absent. Hence we can study production (linear inertial) and rapid pressure effects in relative isolation. The rapid pressure-strain correlation which

---

This thesis follows the style of Physical Review E.

represents the pressure effect in RD limit plays a crucial role in the dynamics of complex turbulent flows. The linearity of governing equations also leads to considerable computational ease in numerically solving the evolution equations. It is interesting to note that in the rapid distortion limit, the fluctuating velocity field exhibits elastic behavior – Reynolds stress is proportional to mean strain – instead of viscous behavior where stress is proportional to strain-rate.

The RDT equations contain both the inertial effects and pressure effects. In an attempt to completely isolate the pressure effects, the RD equations are further simplified. When the pressure term is dropped from the RD equations we are left with the inviscid 3D Burgers equations in RD limit. The ensuing set of equations constitutes what we call the RDT-B model. Burgers equation, despite their inherent simplicity, has been found to duplicate important turbulence phenomena [1]. In fact Burgers equation has been proposed as a simple model foe compressible turbulence [2]. It should be noted that incompressibility constraint is not satisfied in RDT-B model as the pressure term is absent. Comparison between RDT-B and RDT results will provide valuable insight into some aspects of compressible turbulence and the role played by rapid pressure term in incompressible turbulence. We also present a third set of equations, designated as RDT-BC, with incompressibility enforced artificially at each time step during computations of Burgers equations. It is demonstrated that resultant Reynolds stress evolution from RDT-BC calculation is identical to Navier-Stokes RDT. This implies that the role of rapid

pressure term in incompressible turbulence is to merely impose incompressibility in a manner given by the correction term.

The objective of the study is to better understand the role of pressure and inertial effects in turbulence dynamics using simplified equations or models. An improved understanding of these processes is expected to lead to the development of more accurate and realistic models for rapid pressure-strain correlation in future. In this work, the response of initially isotropic and anisotropic homogeneous turbulence flow subjected to different types of strain-dominated and rotation-dominated mean flow fields is studied. We specifically study the following cases of initial anisotropy of turbulence: axisymmetric two-component and initially isotropic turbulence.

1.2 Velocity gradient dynamics

Many aspects of the non-linear turbulence cascade are well captured by Burgers equations. Girimaji and Zhou [1] demonstrate that the triadic interactions in one-dimensional (1D) Burgers equations are quite similar to that in three-dimensional (3D) turbulence. This is despite the fact that both energy and enstrophy are inviscid invariants in the former whereas only energy is conserved in the latter. The probability density functions (PDFs) of velocity and velocity gradients obtained from Burgers equations also share similarities with those from Navier-Stokes equations [3, 4]. Another reason for interest in Burgers equation is the fact that it constitutes a fairly accurate model of

compressible turbulence in the high Mach number limit [2]. Thus, despite its simplicity, Burgers equations can offer valuable insight into turbulence physics.

In this work, we will investigate further aspects of velocity gradient dynamics in Burgers turbulence. Velocity gradient dynamics offer important insight into many turbulent processes such as vortex-stretching and material element straining. Vieillefosse [5] was among the first to study velocity gradient evolution using a simple autonomous dynamical system of equations called restricted Euler equations. These equations are obtained by neglecting the anisotropic pressure Hessian ($H_{ij} = 0$) in the Euler velocity gradient equations. Vieillefosse performed approximate asymptotic analysis of restricted Euler equations and two important observations were made concerning the geometry of velocity gradient tensor: (i) two of the eigenvalues of strain-rate tensor are positive and one is negative with the intermediate eigenvalue having smaller magnitude compared to the other two and (ii) vorticity is aligned with the intermediate eigenvector. Cantwell [6] developed more detailed solutions of the restricted Euler equation and compared the results with isotropic DNS data. Invariant maps which facilitate the study of velocity gradient geometry were introduced in this work. Girimaji and Speziale [7] developed the modified restricted Euler equation that can be used for flows with non-zero mean velocity gradient. The effect of viscosity on the evolution of velocity gradients is addressed by Jeong and Girimaji [8].

The objective of our work is to examine the behavior of velocity gradients in Burgers turbulence. The results will be compared with restricted Euler equation calculations. It is noted that inviscid 3D Burgers equations and restricted Euler equations differ only by the absence of pressure term in the former. Therefore incompressibility condition is not satisfied in case of Burgers equations. A comparison of results from Burgers and Restricted Euler equations will help us characterize the inertial and pressure effects on the nonlinear velocity gradient dynamics in incompressible turbulence and provide insight into energy cascade in compressible turbulence.

In this study, exact asymptotic solutions to both Burgers and restricted Euler equations are studied using fixed point analysis. Numerical computations are then performed to isolate the stable solutions from the complete set of fixed points. The analytical solutions are then used to study the properties of velocity gradient tensor in the asymptotic limit. In particular, we are interested in the three main features: (i) The sign of intermediate principle strain-rate tensor, (ii) alignment of vorticity and (iii) the direction and rate of energy cascade. We will study these issues at the stable analytical solutions of both Burgers and restricted Euler equations. The results from the two approaches are compared to isolate the effect of pressure. Finally, we present third category of equations – the restricted Burgers equations – where the evolution of anisotropic part of the Burgers velocity gradient tensor is examined. As the anisotropic part of the velocity gradient tensor is inherently traceless, this is equivalent to imposing incompressibility on

Burgers calculations. We compare the numerical computations of restricted Burgers equation with those of the restricted Euler equation.

CHAPTER II

INERTIAL AND PRESSURE EFFECTS IN THE RAPID DISTORTION LIMIT

2.1 Governing equations

In this chapter, we present the Navier-Stokes and 3D Burgers equations in the inviscid RD limit. We also consider a third category of equations called the corrected Burgers system in which incompressibility is artificially imposed.

2.1.1 Navier-Stokes RDT equations

The RDT equations are obtained from the complete Navier-Stokes equations given by

$$\frac{\partial V_j}{\partial t} + V_i \frac{\partial V_j}{\partial x_i} = -\frac{1}{\rho}\frac{\partial P}{\partial x_j} + \upsilon \frac{\partial^2 V_j}{\partial x_i \partial x_i}, \tag{2.1}$$

where $V(\vec{x},t)$, $P(\vec{x},t)$ are the instantaneous velocity field and pressure respectively. The velocity field and pressure field are decomposed into mean and fluctuating components

$$\tilde{U}(\vec{x},t) = U(\vec{x},t) + u(\vec{x},t), \tag{2.2}$$

$$P(\vec{x},t) = \overline{P}(\vec{x},t) + p(\vec{x},t).$$

Substituting this decomposition in the Navier-Stokes equations and taking mean of the resulting equations, we get the evolution equations for mean velocity component, referred to as Reynolds Averaged Navier-Stokes (RANS) equations

$$\frac{\overline{D}U_j}{Dt} = -\frac{1}{\rho}\frac{\partial \overline{P}}{\partial x_j} + \upsilon\frac{\partial^2 U_j}{\partial x_i \partial x_i} - \frac{\partial \langle u_i u_j \rangle}{\partial x_i}, \tag{2.3}$$

where

$$\frac{\overline{D}}{\overline{D}t} = \frac{\partial}{\partial t} + U_i \frac{\partial}{\partial x_i}.$$

$\langle u_i u_j \rangle$ is the Reynolds stress and angular brackets imply summation. The evolution equation for fluctuating velocity field is obtained by subtracting RANS from the full Navier-Stokes equations. In homogeneous turbulence, this equation simplifies to

$$\frac{\overline{D}u_j}{Dt} = -\frac{1}{\rho}\frac{\partial p}{\partial x_j} + \upsilon\frac{\partial^2 U_j}{\partial x_i \partial x_i} - u_i\frac{\partial u_j}{\partial x_i} - u_i\frac{\partial U_j}{\partial x_i}. \tag{2.4}$$

The fluctuating pressure (p) is governed by Poisson equation

$$\frac{1}{\rho}\nabla^2 p = -2\frac{\partial U_i}{\partial x_j}\frac{\partial u_j}{\partial x_i} - \frac{\partial u_i}{\partial x_j}\frac{\partial u_j}{\partial x_i}. \tag{2.5}$$

Now, pressure is decomposed into two components – rapid pressure ($p^{(r)}$) and slow pressure ($p^{(s)}$) so that

$$\frac{1}{\rho}\nabla^2 (p^{(r)} + p^{(s)}) = -2\frac{\partial U_i}{\partial x_j}\frac{\partial u_j}{\partial x_i} - \frac{\partial u_i}{\partial x_j}\frac{\partial u_j}{\partial x_i}. \tag{2.6}$$

The first term on the right-hand side is linear in fluctuating velocity and it accounts for the interactions between mean flow and the turbulent fluctuations whereas the second

term is nonlinear and it represents the turbulence-turbulence interactions. In the RD limit, the mean velocity gradients $\left(\frac{\partial U_i}{\partial x_j}\right)$ are assumed to be much larger than the fluctuating velocity gradients $\left(\frac{\partial u_i}{\partial x_j}\right)$. Thus, turbulence-turbulence interactions can be neglected and hence Eqs. (2.4) and (2.6) reduce to the *rapid distortion equations* [9]

$$\frac{\overline{D}u_j}{\overline{D}t} = -u_i \frac{\partial U_j}{\partial x_i} - \frac{1}{\rho}\frac{\partial p^{(r)}}{\partial x_j}; \tag{2.7}$$

$$\frac{1}{\rho}\nabla^2 p^{(r)} = -2\frac{\partial U_i}{\partial x_j}\frac{\partial u_j}{\partial x_i}. \tag{2.8}$$

The first term on the right-hand side of Eq. (2.7) represents the inertial effect and the second term refers to the pressure effect. It is noted that the equations are linear in fluctuating velocity. The incompressibility condition on the fluctuating velocity is given by

$$\frac{\partial u_i}{\partial x_i} = 0. \tag{2.9}$$

These equations can be solved most conveniently in Fourier space, an approach first introduced by Taylor and Batchelor (1949). In this approach, velocity and pressure are represented as sum of a finite number of Fourier modes:

$$u(\vec{x},t) = \sum_{\vec{k}} \hat{u}(\vec{\kappa},t) e^{i\vec{\kappa}(t)\cdot\vec{x}}, \quad p^{(r)}(\vec{x},t) = \sum_{\vec{k}} \hat{p}(t) e^{i\vec{\kappa}(t)\cdot\vec{x}}. \tag{2.10}$$

where $\vec{\kappa}(t)$ is the wavenumber vector and $\hat{u}(\vec{\kappa},t)$, $\hat{p}(t)$ are the corresponding Fourier coefficients. As the equations are linear, each Fourier mode evolves independently and

hence the equations can be decomposed and written for each fluctuation mode separately. The equations in Fourier space for each mode are given by [9]:

$$\frac{d\kappa_l}{dt} = -\kappa_j \frac{\partial U_j}{\partial x_l}; \tag{2.11}$$

$$\frac{d\hat{u}_j}{dt} = -\hat{u}_k \frac{\partial U_l}{\partial x_k}\left(\delta_{jl} - 2\frac{\kappa_j \kappa_l}{\kappa^2}\right), \tag{2.12}$$

and the incompressibility constraint is given by

$$\hat{u}_i k_i = 0. \tag{2.13}$$

Eq. (2.13) indicates that the wavenumber vector $\vec{\kappa}(t)$ and velocity vector $\hat{u}(\vec{\kappa},t)$ are orthogonal to each other at all times. Given the initial conditions and the mean flow gradients, equations (2.11), (2.12) and (2.13) can be solved numerically.

The wavenumber vector can be decomposed as $\vec{\kappa}(t) = \kappa(t)\vec{e}(t)$, where $\kappa(t)$ is the magnitude and $\vec{e}(t)$ is the unit vector corresponding to $\vec{\kappa}(t)$.Now, Eqs. (2.11) and (2.12) can be rewritten as

$$\frac{de_l}{dt} = -\frac{\partial U_m}{\partial x_i} e_m\left(\delta_{il} - e_i e_l\right); \tag{2.14}$$

$$\frac{du_j}{dt} = -u_k \frac{\partial U_l}{\partial x_k}\left(\delta_{jl} - 2e_j e_l\right). \tag{2.15}$$

It can be seen that the equations contain only the unit vector corresponding to each wavenumber vector and there is no dependence on its magnitude ($\kappa(t)$). Hence, the

evolution of the unit wavenumber vector $\vec{e}(t)$ can be treated as the trajectory on a unit sphere. The covariance of Fourier coefficients conditioned on a given wavenumber is:

$$\hat{R}_{ij}(\vec{\kappa},t) = \left\langle \hat{u}_i^*(\vec{\kappa},t), \hat{u}_j(\vec{\kappa},t) \right\rangle . \tag{2.16}$$

This is an important quantity of interest as the Reynolds stresses in physical space can be obtained by:

$$\left\langle u_i u_j \right\rangle = \sum_{\vec{k}} \hat{R}_{ij}(\vec{\kappa},t) . \tag{2.17}$$

Thus $\hat{R}_{ij}(\vec{\kappa},t)$ can be interpreted as the Reynolds stress conditioned on a given wavenumber vector. We can write the evolution equation for $\hat{R}_{ij}$ using Eqs. (2.11) and (2.12) (See [9] for complete details of derivation)

$$\frac{d\hat{R}_{ij}}{dt} = -\hat{R}_{ik}\frac{\partial U_j}{\partial x_k} - \hat{R}_{jk}\frac{\partial U_i}{\partial x_k} + 2\hat{R}_{ik}\frac{\partial U_l}{\partial x_k}\frac{\kappa_j\kappa_l}{\kappa^2} + 2\hat{R}_{jk}\frac{\partial U_l}{\partial x_k}\frac{\kappa_i\kappa_l}{\kappa^2} . \tag{2.18}$$

Incompressibility equation can be rewritten as

$$\kappa_i \hat{R}_{ij}(\vec{\kappa},t) = \kappa_j \hat{R}_{ij}(\vec{\kappa},t) = 0 . \tag{2.19}$$

For evaluating Reynolds stresses, solving Eqs. (2.11), (2.18) and (2.19) is numerically more efficient alternative to solving Eqs. (2.11)-(2.13) [10]. Hence (2.11, 2.18, 2.19) constitute the RDT equations employed in our computations.

Using Eqs. (2.17) and (2.18), the evolution equation for Reynolds stresses can be written as:

$$\frac{d\left\langle u_i u_j \right\rangle}{dt} = P_{ij} + \Phi_{ij}^{(r)} , \tag{2.20}$$

where Production P_{ij} is given by

$$P_{ij} = -\sum_{\vec{k}} \left(\hat{R}_{ik} \frac{\partial U_j}{\partial x_k} + \hat{R}_{jk} \frac{\partial U_i}{\partial x_k} \right)$$

and rapid pressure strain correlation $\Phi_{ij}^{(r)}$ is defined as

$$\Phi_{ij}^{(r)} = 2\sum_{\vec{k}} \left(\hat{R}_{ik} \frac{\partial U_l}{\partial x_k} \frac{\kappa_j \kappa_l}{\kappa^2} + 2\hat{R}_{jk} \frac{\partial U_l}{\partial x_k} \frac{\kappa_i \kappa_l}{\kappa^2} \right).$$

These equations completely describe the evolution of Reynolds stresses in the RD limit.

In our study we focus on the Reynolds stress anisotropy tensor (b_{ij}):

$$b_{ij} = \frac{\langle u_i u_j \rangle}{2k} - \frac{1}{3}\delta_{ij}, \tag{2.21}$$

where δ_{ij} is the *kronecker delta* and the turbulent kinetic energy (k) is given by

$$k = \frac{1}{2}\langle u_i u_i \rangle .$$

We also study the evolution of anisotropy invariants:

$$\eta = \left(\frac{1}{6} b_{ij} b_{ji} \right)^{1/2} ; \; \xi = \left(\frac{1}{6} b_{ij} b_{jk} b_{ki} \right)^{1/3} . \tag{2.22}$$

2.1.2 RDT-B equations

The full 3D Burgers equation is given by

$$\frac{dV_j}{dt} + V_i \frac{dV_j}{dx_i} = \upsilon \frac{\partial^2 V_j}{\partial x_i \partial x_i} . \tag{2.23}$$

Comparing the forms of equation (2.23) and (2.1) it can be seen that Burgers equation is pressure-less version of Navier-Stokes equation. The inertial and viscous effects are retained intact in Burgers equations. The difference between solutions to Navier-Stokes and Burgers equations can be attributed to the pressure field. The Burgers equations in the inviscid RD limit can be simply obtained by dropping the pressure term from full RDT equations. The resulting equations, which we call RDT-B equations, are

$$\frac{de_l}{dt} = -\frac{\partial U_m}{\partial x_i} e_m \left(\delta_{il} - e_i e_l\right); \tag{2.24}$$

$$\frac{\overline{D}\hat{u}_j}{\overline{D}t} = -\hat{u}_k \frac{\partial U_j}{\partial x_k};$$

The corresponding conditioned Reynolds stress equation is

$$\frac{d\hat{R}_{ij}}{dt} = -\hat{R}_{ik} \frac{\partial U_j}{\partial x_k} - \hat{R}_{jk} \frac{\partial U_i}{\partial x_k}. \tag{2.25}$$

The Reynolds stress evolution equation in physical space is

$$\frac{d\left\langle u_i u_j \right\rangle}{dt} = P_{ij}. \tag{2.26}$$

Thus, in the absence of pressure, wavenumber plays no role in the velocity field evolution and Reynolds stress evolution is dictated solely by production. Most importantly, the incompressibility condition is not satisfied,

$$\kappa_i \hat{R}_{ij}(\vec{\kappa}, t) \neq 0; \quad \kappa_j \hat{R}_{ij}(\vec{\kappa}, t) \neq 0. \tag{2.27}$$

Notwithstanding the effects of incompressibility, the difference between RDT-B and RDT results will highlight the role of rapid pressure-strain correlation in turbulence evolution

2.1.3 Corrected Burgers equation

The biggest shortcoming of the Burgers equation is clearly its inability to preserve the incompressibility constraint. To overcome this deficiency, we propose a simple correction to the Burgers solution:

$$\left(\hat{R}_{ij}(\hat{k},t)\right)_{RDT-BC} = \left(\hat{R}_{lm}(\hat{k},t)\right)_{RDT} \cdot \left(\delta_{il} - e_i e_l\right)\left(\delta_{jm} - e_j e_m\right) \tag{2.28}$$

where $\vec{e}(t)$ evolves according to Eq. (2.14). The $\hat{R}_{ij}$ thus obtained will preserve the incompressibility requirement. In spectral space, this correction effectively means that $\hat{R}_{ij}$ is being projected on to a plane perpendicular to the corresponding wavenumber vector so that equation (2.19) is satisfied. The results from this set of calculations are denoted as RDT-BC.

2.2 Numerical implementation

The RDT equations (Eqs. 2.11, 2.18 and 2.19) are computed numerically using a fourth order Runge-Kutta scheme. The Reynolds stress evolution is then obtained for various mean flow conditions and initial turbulence states. Subsequently, all the required quantities such as anisotropy tensor (b_{ij}) and its invariants (ζ,η) are evaluated. It should be cautioned here that RD results represent a limiting state of turbulence only for a limited period of time. Nevertheless, to clearly understand linear physics, we perform computations until asymptotic state is reached.

The code used is very similar to the one presented in [11]. A switch is additionally incorporated that enables us to turn on and off the rapid pressure term, thus simulating the RDT-B as well. The different types of homogeneous 2D mean flow conditions considered in our study are

Case 1 – Homogeneous shear

$$\frac{dU_i}{dx_j} = S\begin{bmatrix} 0 & 1 & 0 \\ 0 & 0 & 0 \\ 0 & 0 & 0 \end{bmatrix} \tag{2.29}$$

Case 2 – Strain Dominated flow (Plane Strain)

$$\frac{dU_i}{dx_j} = S\begin{bmatrix} 1 & 0 & 0 \\ 0 & -1 & 0 \\ 0 & 0 & 0 \end{bmatrix}$$

Case 3 – Strain Dominated flow

$$\frac{dU_i}{dx_j} = S\begin{bmatrix} 0 & 0.7 & 0 \\ 0.1 & 0 & 0 \\ 0 & 0 & 0 \end{bmatrix}$$

Case 4 – Rotation Dominated Flow

$$\frac{dU_i}{dx_j} = S\begin{bmatrix} 0 & 0.7 & 0 \\ -0.1 & 0 & 0 \\ 0 & 0 & 0 \end{bmatrix}$$

Case 5 – Rotation Dominated Flow

$$\frac{dU_i}{dx_j} = S\begin{bmatrix} 0.3 & 0.4 & 0 \\ -0.4 & -0.3 & 0 \\ 0 & 0 & 0 \end{bmatrix}$$

Where $S = \sqrt{S(t) \bullet S(t)}$

The term *S* can be viewed as the frequency and its reciprocal the characteristic timescale of mean flow. Without loss of generality, we set $S = 1$ in all our calculations. A mean flow is classified as strain-dominated or rotation-dominated based on the magnitudes of $S_{ij}S_{ij}$ and $R_{ij}R_{ij}$:

$$\beta = \frac{R_{ij}R_{ij}}{R_{ij}R_{ij} + S_{ij}S_{ij}} \tag{2.30}$$

Hence $0 \le \beta < 0.5$ corresponds to the strain dominated flows, with $\beta = 0$ representing the plane strain mean flow; $\beta = 0.5$ representing the shear mean deformation case; $0.5 < \beta \le 1$ corresponds to the rotation-dominated flow regime and $\beta = 1$ represents the vortical flow. Rotation-dominated flows are also referred to as elliptic flows in literature. This is due to the fact that mean streamlines in such flows are elliptic in shape.

Four different types of initial anisotropy conditions of turbulence have been used in this study – three different axisymmetric two-component (2C) states and the isotropic initial state. The corresponding anisotropy tensors are given by:

$$b_{ij} = \begin{bmatrix} -1/3 & 0 & 0 \\ 0 & 1/6 & 0 \\ 0 & 0 & 1/6 \end{bmatrix}; \quad b_{ij} = \begin{bmatrix} 1/6 & 0 & 0 \\ 0 & -1/3 & 0 \\ 0 & 0 & 1/6 \end{bmatrix}; \tag{2.31}$$

$$b_{ij} = \begin{bmatrix} 1/6 & 0 & 0 \\ 0 & 1/6 & 0 \\ 0 & 0 & -1/3 \end{bmatrix} \text{ and } b_{ij} = \begin{bmatrix} 0 & 0 & 0 \\ 0 & 0 & 0 \\ 0 & 0 & 0 \end{bmatrix}.$$

The first three states are designated as 2C1, 2C2 and 2C3 respectively. The final b_{ij} corresponds to the isotropic (ISO) initial condition.

Many different choices of wavenumber vectors and Fourier coefficients yield the aforementioned initial conditions. But we need to choose an initial velocity field that is completely unbiased in terms of wavenumber distributions and directional preference. The following assumptions are made in determining the initial wavenumber ($\vec{\kappa}(t=0)$) and velocity vector ($\vec{u}(\vec{\kappa},t=0)$) [11]

(a) The velocity fluctuations in all permissible directions are uniform. Permissible directions are determined from the initial anisotropy of the Reynolds stress tensor.

(b) For a given velocity vector $\vec{u}(\vec{\kappa},t=0)$ all permissible wavenumber vector directions are equally probable. Permissible wavenumber vector directions are determined subject to the incompressibility condition (Eq. 2.13).

For instance, to generate an isotropic initial condition, the initial velocity vectors $\vec{u}(\vec{\kappa},t=0)$ are uniformly distributed all over a unit sphere. As the evolution doesn't depend on the magnitude of wavenumber vector, without any loss of generality, we can assume that all the initial wavenumber vectors are of equal magnitude. Hence, for isotropic initial condition the wavenumber vectors are uniformly distributed over the surface of unit sphere. 2C initial conditions can also be generated using similar logic (See [11] for more details).

2.3 Results and analysis

The RD calculations are performed for all the different combinations of mean flows and initial conditions mentioned earlier. The results are presented in four parts: (i) the kinetic energy evolution is examined for different values of β with isotropic initial condition; (ii) we study the evolution of anisotropy tensor as a function of β with the initial condition of turbulence being isotropic; (iii) the effect of varying the initial condition is investigated; and (iv) finally, the results from RDT-BC computations are presented to further quantify the effect of rapid pressure term.

2.3.1 Evolution of turbulent kinetic energy

The evolution of turbulent kinetic energy for several strain-dominated mean flows is shown in Fig. 1. In strain-dominated flows, RDT suggests that kinetic energy settles down to an asymptotic state after some time whereas RDT-B predicts a monotonic growth for kinetic energy. In the asymptotic state predicted by RDT $\langle u_1 u_1 \rangle, \langle u_2 u_2 \rangle$ and $\langle u_1 u_2 \rangle$ are identically equal to zero and all the kinetic energy is contained in $\langle u_3 u_3 \rangle$ component. Therefore production (P_{ii}) becomes zero once the asymptotic state is reached and consequently kinetic energy remains constant. In the absence of pressure (RDT-B) $\langle u_1 u_1 \rangle, \langle u_2 u_2 \rangle$ and $\langle u_1 u_2 \rangle$ are finite in the asymptotic limit hence and production remains nonzero at all times. As a result, we have continuous kinetic energy growth.

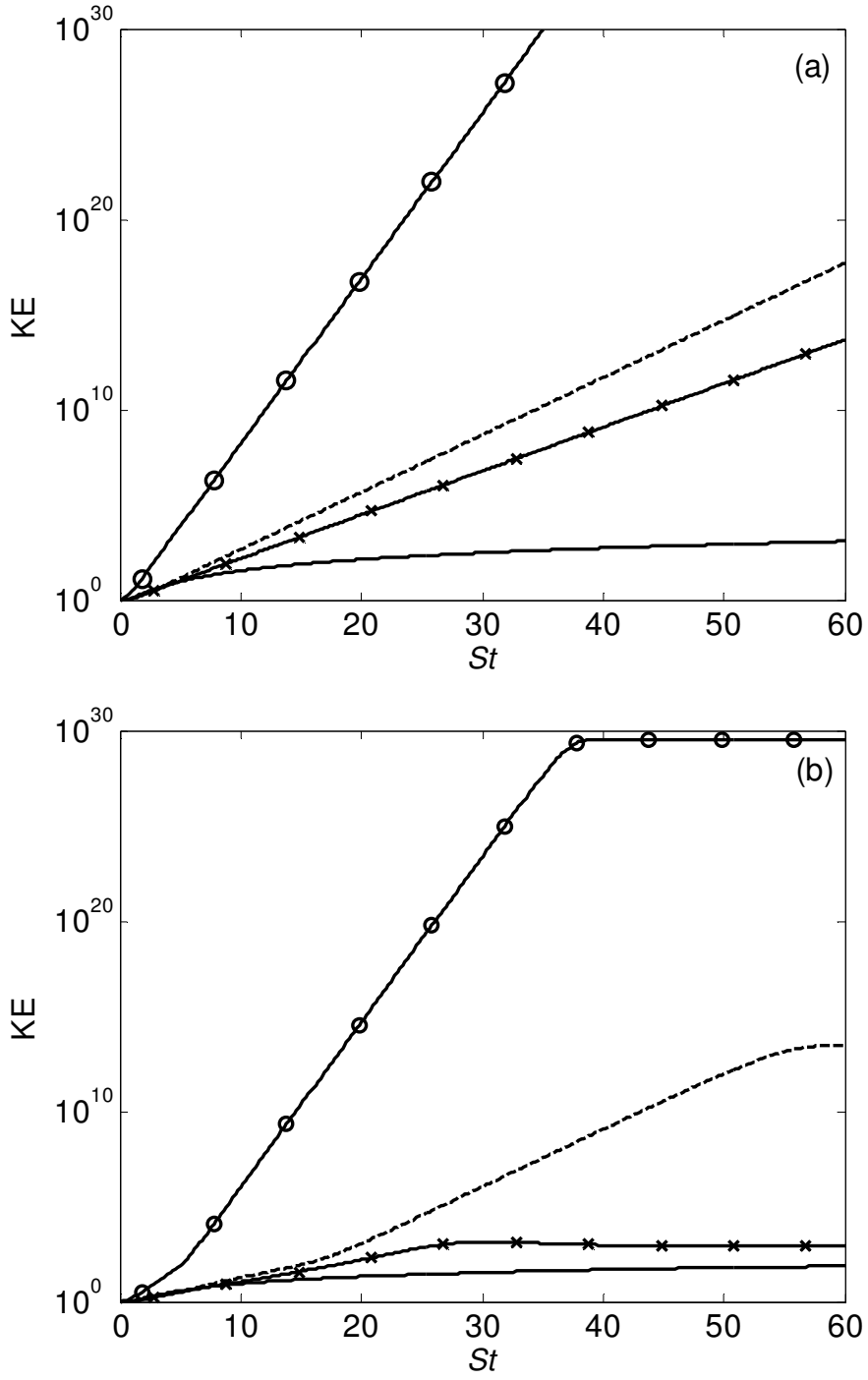

FIG. 1. Evolution of kinetic energy for strain-dominated flows with different β. (a) RDT-B and (b) RDT. Legend: (–o–) $\beta = 0$, (––) $\beta = 0.2$, (–x–) $\beta = 0.36$, (—) $\beta = 0.5$.

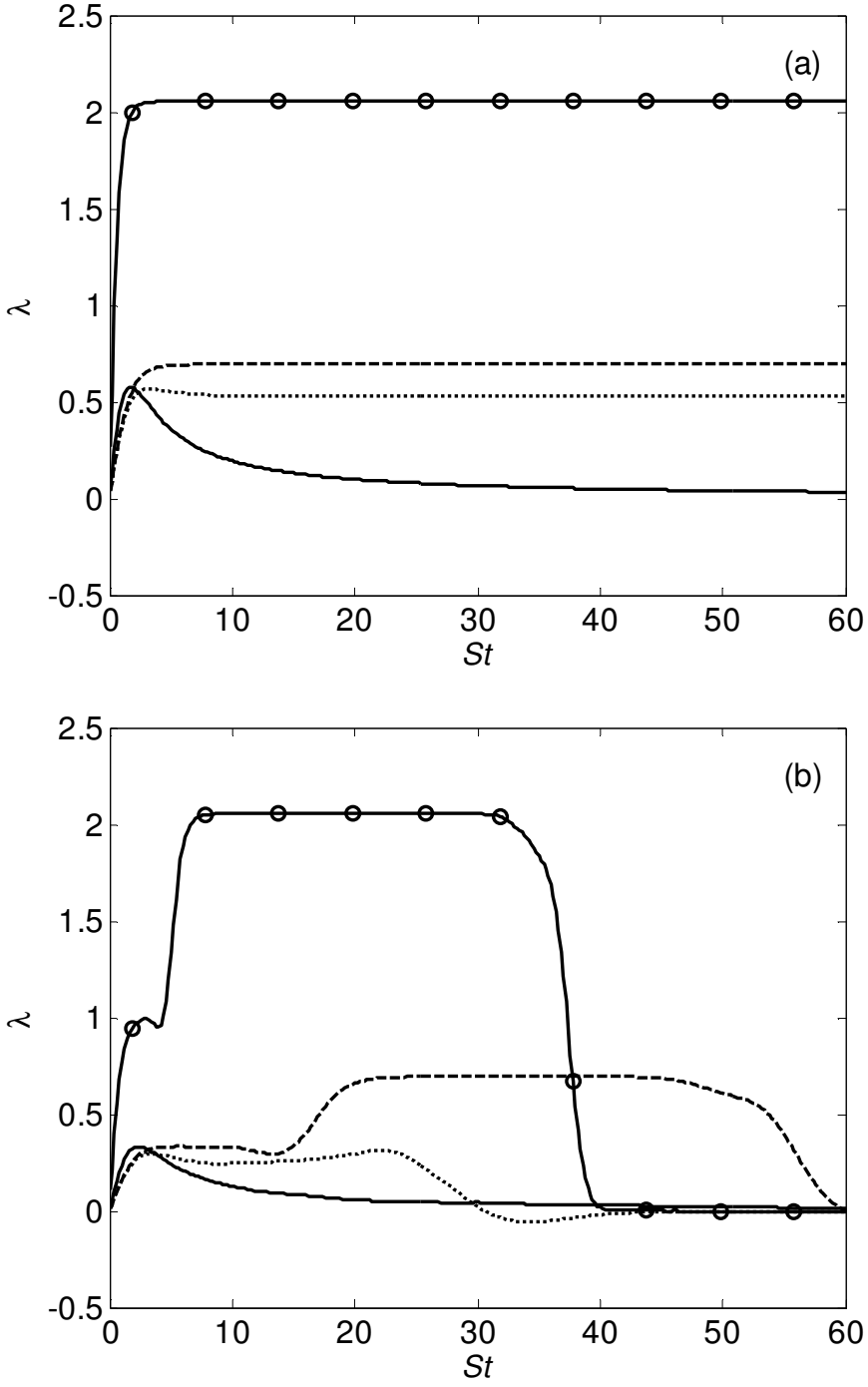

FIG. 2. Evolution of λ for the strain-dominated mean flows with different β. (a) RDT-B and (b) RDT. Legend: (–o–) $\beta = 0$, (▬▬) $\beta = 0.2$, (•••) $\beta = 0.36$, (—) $\beta = 0.5$.

Kinetic energy evolution can also be examined in terms of its growth rate (λ) defined as:

$$\lambda = \frac{1}{k}\frac{dk}{dt}. \tag{2.32}$$

In Fig. 2, the growth rate indeed goes to zero in the asymptotic limit in case of RDT whereas RDT-B predicts a constant growth rate. Thus, in strain-dominated flows, the net effect of pressure is moderate the growth of kinetic energy to some extent and eventually stop the growth in the asymptotic limit.

In rotation-dominated flows, we find kinetic energy grows continuously to large magnitudes in case of RDT (Fig. 3). But RDT-B predicts a periodic oscillating evolution with much lower magnitudes of kinetic energy. Thus the effect of pressure in rotation-dominated flows is exact opposite of what is seen in strain-dominated flows. In order to investigate this further, we look into the evolution of net production (P_{ii}) for one particular rotation-dominated flow. Taking the trace of Eqn. (2.20), it can easily be shown that rate of change of turbulent kinetic energy is equal to the net production (P_{ii}). From Fig. 4(a) and 4(b), we find that production is always positive and grows monotonically at an increasingly faster rate in case of RDT. This results in the continuous growth of kinetic energy. Without the pressure (RDT-B), production evolves in a periodic manner about zero. Consequently we have periodic evolution of kinetic energy. In effect, it appears that the rapid pressure term reorients the Reynolds stresses such that net production is always positive thus resulting in the continuous growth of

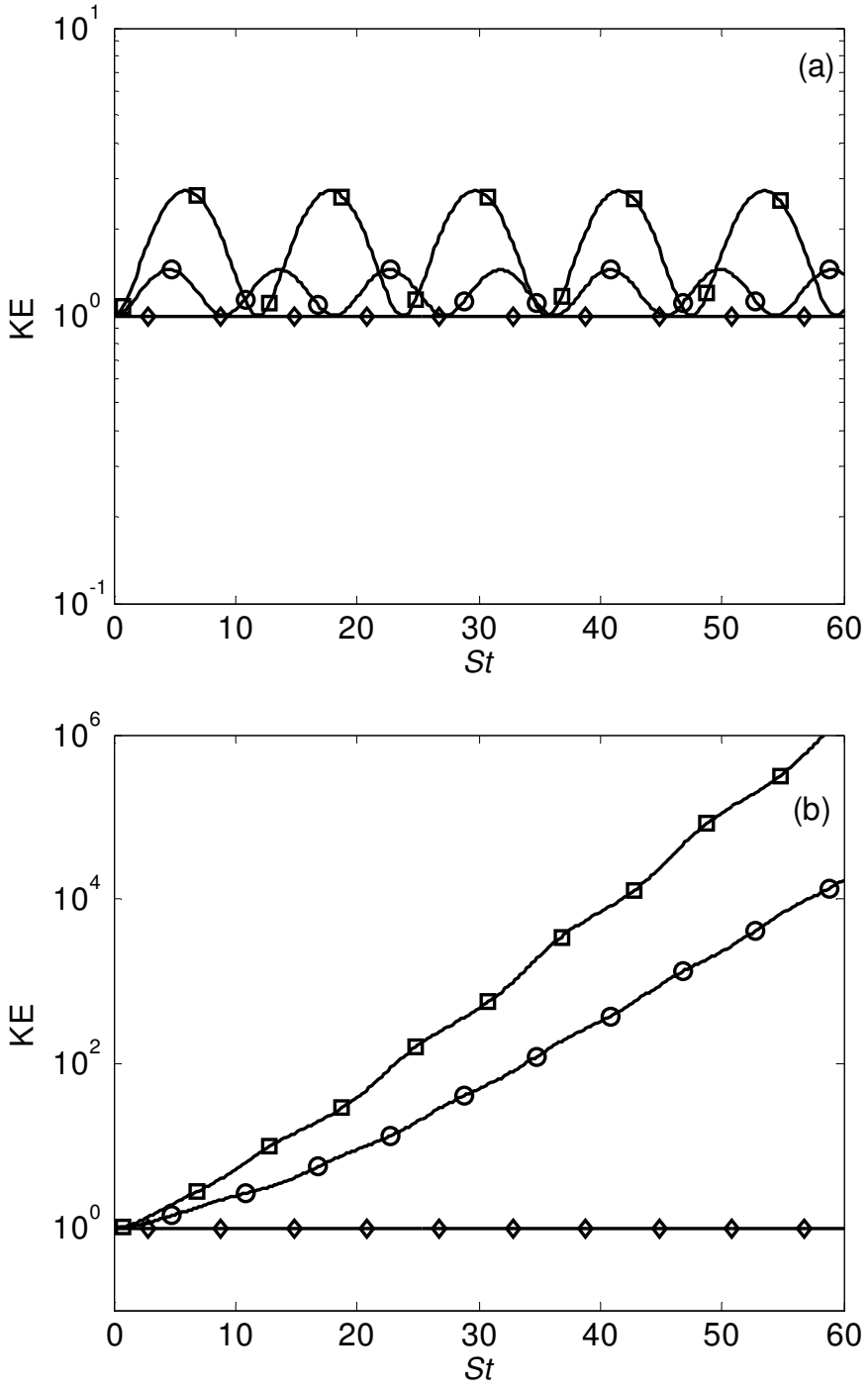

FIG. 3. Evolution of kinetic energy for rotation-dominated flows with different β. (a) RDT-B and (b) RDT. Legend: (–□–) $\beta = 0.64$, (–o–) $\beta = 0.8$, (–◇–) $\beta = 1.0$.

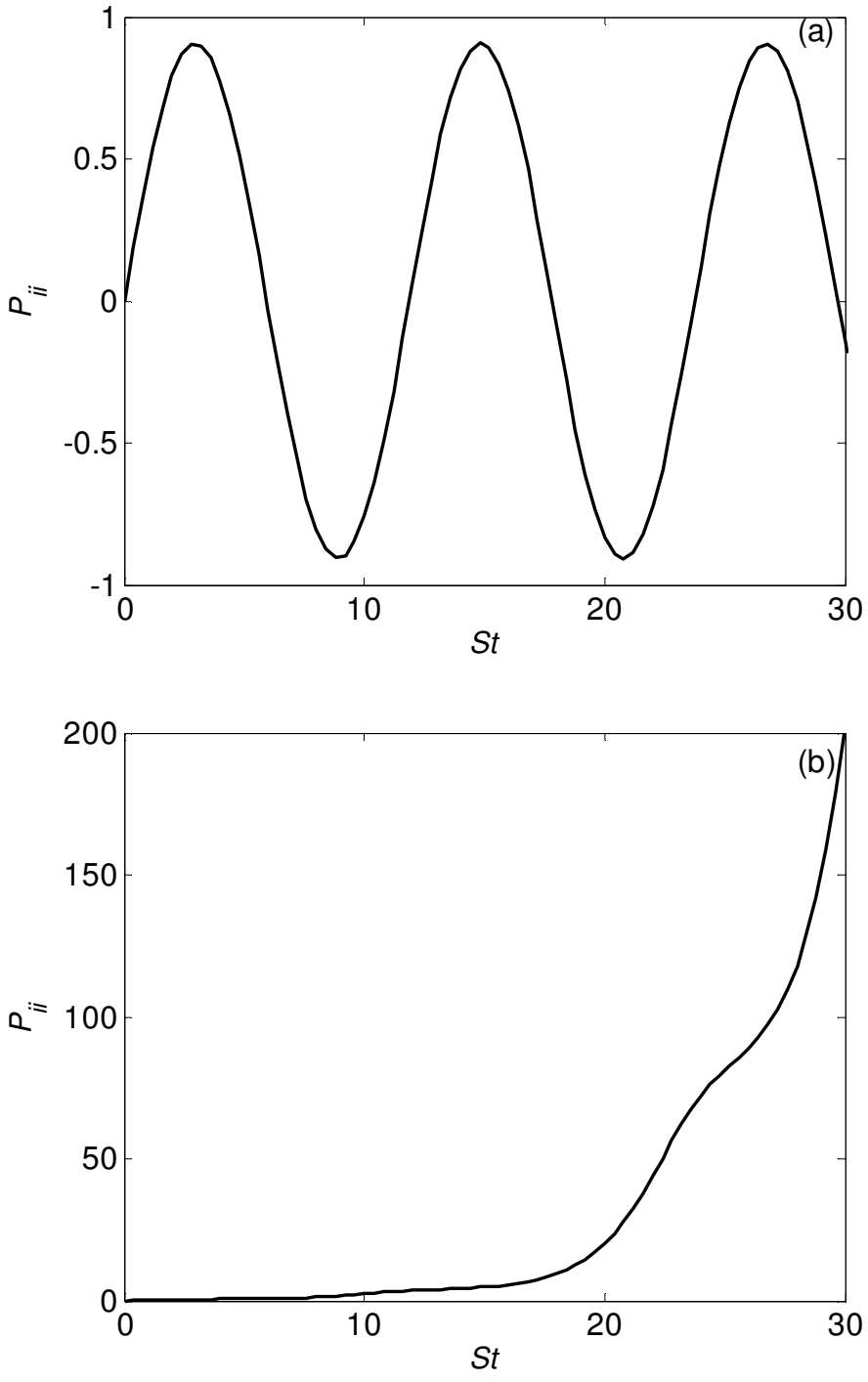

FIG. 4. Evolution of production in a rotation-dominated flow with $\beta = 0.64$.

(a) RDT-B and (b) RDT.

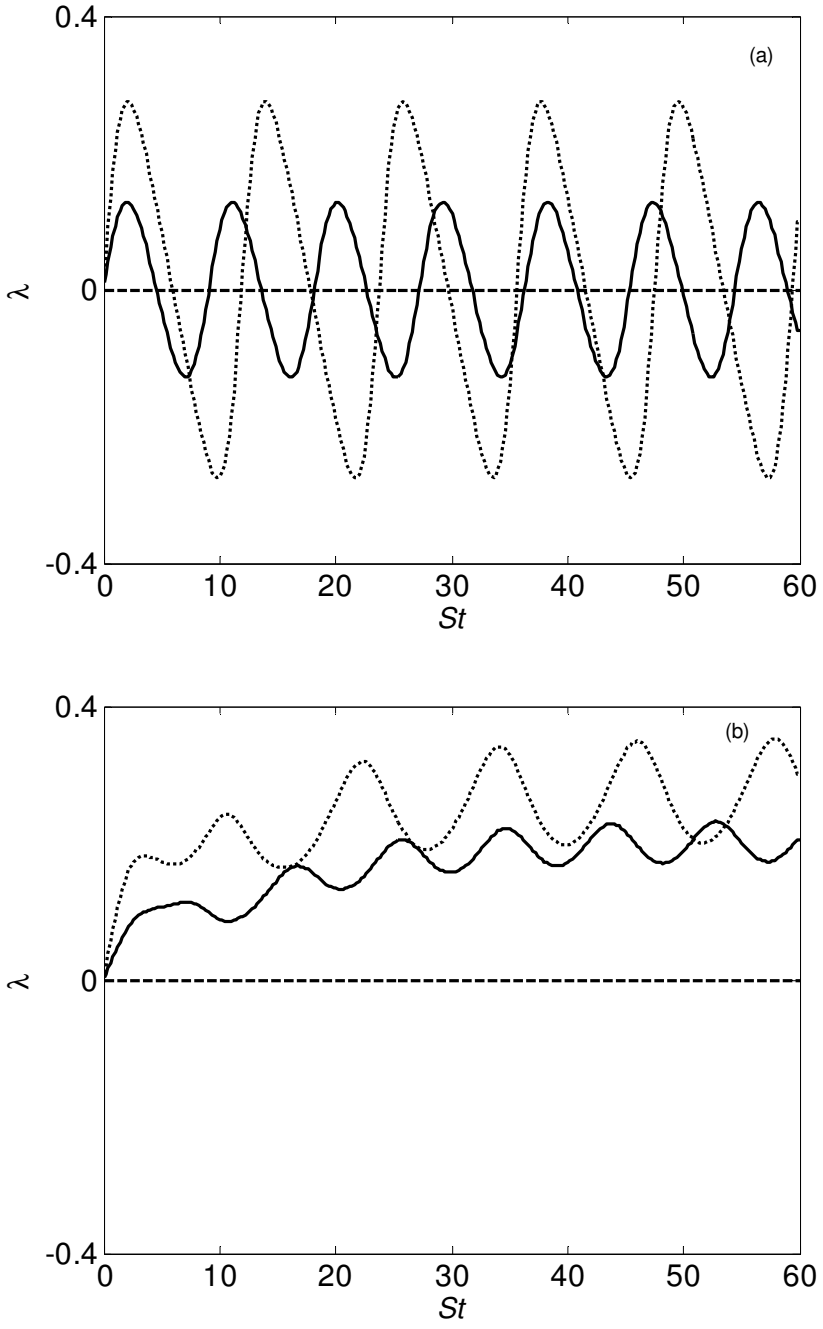

FIG. 5. Evolution of λ for the rotation-dominated mean flows with different β.

(a) RDT-B and (b) RDT. Legend: (•••) $\beta = 0.64$, (▬▬) $\beta = 0.2$, (—) $\beta = 1$.

kinetic energy. The kinetic energy growth rates for different rotation-dominated flows are shown in Fig 5. It should be mentioned that kinetic energy decay noticed in RDT-B results is just a consequence of negative production (Fig. 4) i.e. energy transfer from fluctuating flow to mean flow. This kind of decay of kinetic energy despite the absence of any dissipative mechanism is unusual but not impossible especially in the linear RD limit.

2.3.2 Evolution of anisotropy tensor

The evolution of Reynolds stress anisotropy tensor b_{ij} for several mean flows with different β is studied in this section. The initial condition of turbulence is set to isotropic state in all cases shown here. Figures 6, 7 show the evolution of b_{11} and b_{22} respectively for several different mean flows. The RDT-B and RDT results agree at least in the asymptotic limit in the following cases: (1) Plane Strain ($\beta = 0$), (2) Shear $\beta = 0.5$ and (3) vortical flow ($\beta = 1$). In case of $\beta = 1$, there is no evolution at all; however it is not the case when the initial condition is changed from ISO to one of the three 2C states. In all other intermediate cases, pressure has a definite effect on turbulence anisotropy. In rotation-dominated flows we find that the amplitude of oscillations is considerably damped due to the presence of pressure term. In all strain-dominated cases we find that the pressure term causes the flow to move to an asymptotic state where the Reynolds stresses $\langle u_1 u_1 \rangle$, $\langle u_2 u_2 \rangle$ go to zero and only $\langle u_3 u_3 \rangle$ is energetic

Thus anisotropy goes to the so-called axisymmetric one-componential (1C) limit. As $\langle u_3 u_3 \rangle$ is the only non-zero normal Reynolds stress component, this state is referred to as 1C3. The asymptotic state reached in homogeneous shear flow is also 1C however in this case $\langle u_2 u_2 \rangle$ and $\langle u_3 u_3 \rangle$ are identically equal to zero and $\langle u_1 u_1 \rangle$ is non-zero i.e. 1C1 limit. These aspects can be better observed on a Lumley triangle. The evolution of anisotropy invariants on a Lumley triangle for initially isotropic turbulence subjected to homogeneous shear deformation is shown in Fig. 8. While both the models predict the tendency to move towards the axisymmetric one-componential (1C) limit, RDT-B model predicts a nearly straight trajectory along the axisymmetric one-component line whereas RDT trajectory is highly curved – the flow moves towards the 2C limit initially before going to the 1C limit. Our RDT results for homogeneous shear flow agree with the ones given in [9]. Similar behavior of anisotropy invariants is noticed in the strain-dominated flows also when the initial condition is set to isotropic (Fig 9). However in this case though both RDT-B and RDT eventually go to 1C state the corresponding anisotropy tensors are very different (Fig. 6, 7). An interesting feature noticed in the anisotropy evolution is, in Fig. 7, the sudden drop of b_{22} in case of plane strain mean flow ($\beta = 0$). However this is inevitable as at long times $\hat{\kappa}_2$ tends to infinity causing u_2 to vanish due to the incompressibility constraint

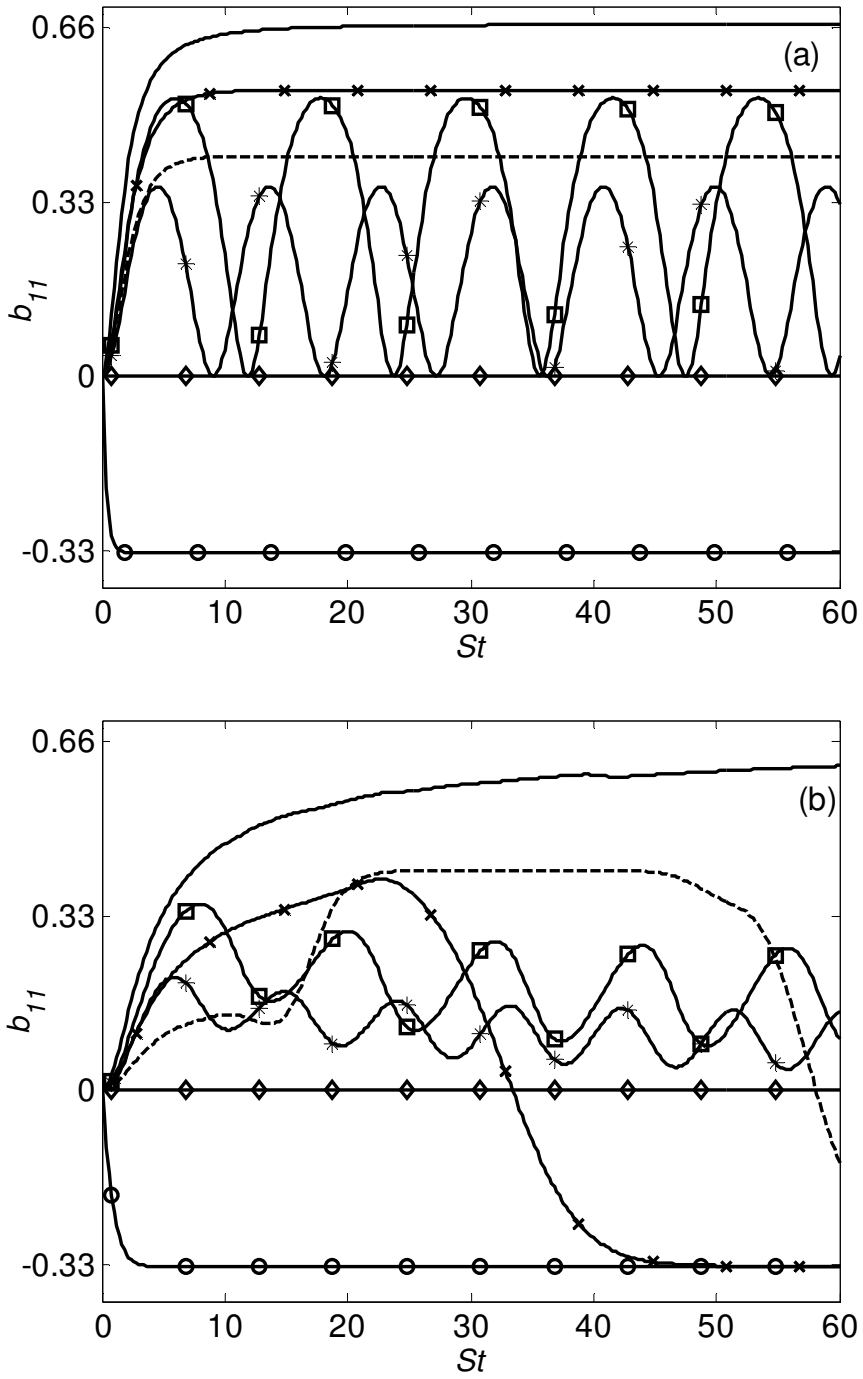

FIG. 6. Evolution of b_{11} for the mean flows with different β. (a) RDT-B and (b) RDT. Legend: (–o–) $\beta = 0$, (––) $\beta = 0.2$, (–x–) $\beta = 0.36$, (—) $\beta = 0.5$, (–□–) $\beta = 0.64$, (–*–) $\beta = 0.8$, (–◊–) $\beta = 1.0$.

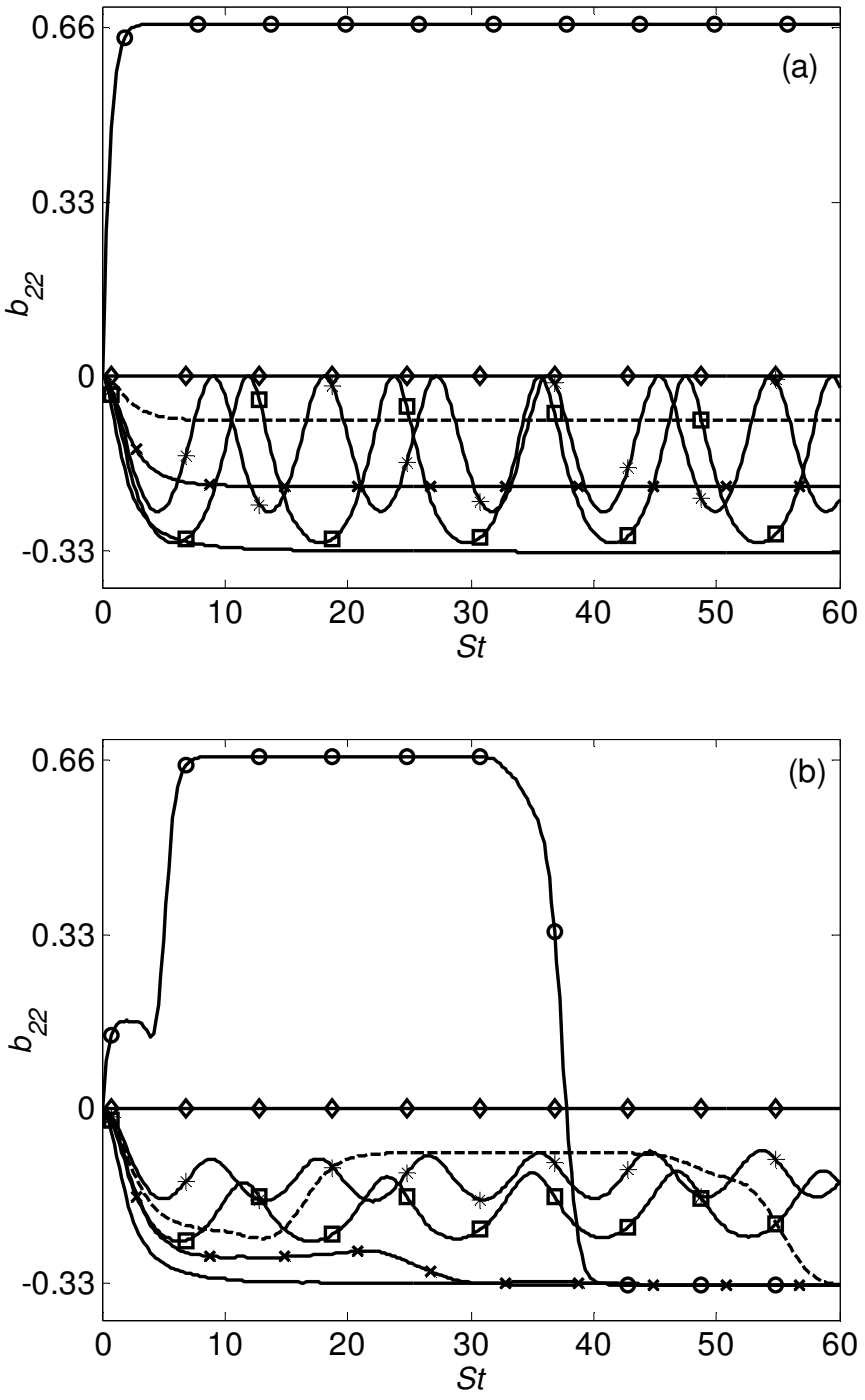

FIG. 7. Evolution of b_{22} for the mean flows with different β. (a) RDT-B and (b) RDT. Legend as given in Fig. 1.

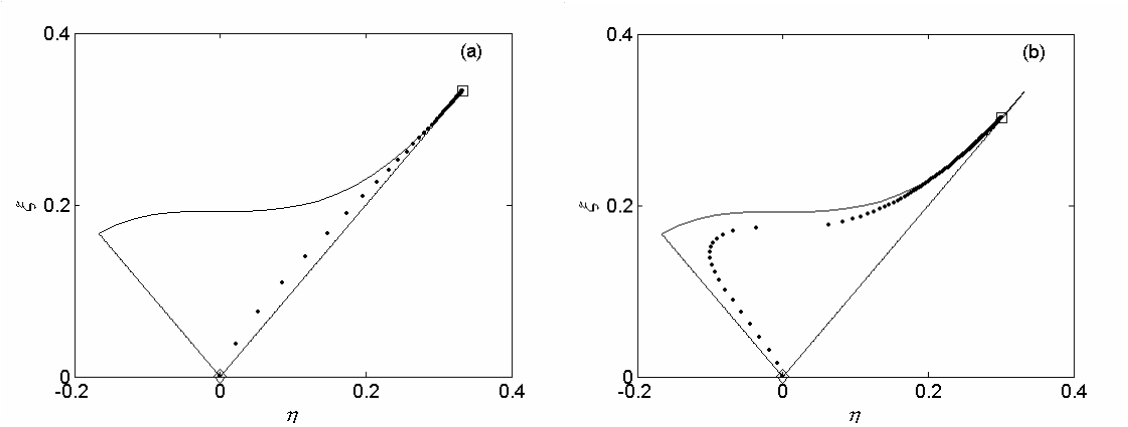

FIG. 8. Lumley triangle for homogeneous shear flow. Initial condition: ISO. (a) RDT-B and (b) RDT. Legend: (◊) – starting point and (□) – end point

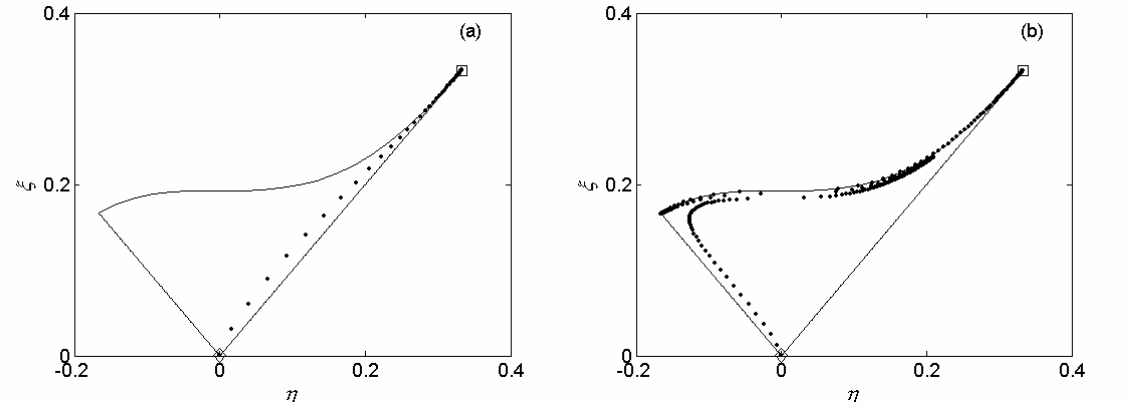

FIG. 9. Lumley triangle for strain-dominated mean flow ($\beta = 0.36$). Initial condition: ISO. (a) RDT-B and (b) RDT. Legend: (◊) – starting point and (□) – end point

2.3.3 Effect of varying initial conditions

In this section, the response of turbulence subjected to various mean flow conditions (given by Eq. 2.29) with anisotropic initial conditions is investigated. The different anisotropic initial conditions defined by Eq. (2.31) are used here. Let us first look at the response of turbulence subjected to homogeneous shear deformation (Case 1). The evolution of Reynolds stress anisotropy tensor (b_{ij}) from 2C1 initial conditions is shown in Fig. 10. Though the predictions are different in the initial times both RDT-B and RDT predict an evolution that settles down to a fixed point in the asymptotic limit. It is found that RDT-B predicts a much faster approach to the fixed point than RDT. The presence of pressure term in RDT slows down the approach to the asymptotic limit. In RDT, the presence of pressure causes the flow to satisfy incompressibility constraint at every stage during its approach to the fixed point whereas no such constraint exists in case of RDT-B. In rapidly distorted homogeneous shear flows it can be said that inertial effects alone dictate the behavior of turbulence in a fairly accurate manner and pressure does not play an important role. But comparing the evolution at early times it can be said that the inertial effects (RDT-B) cause the anisotropy to increase steeply whereas pressure effects counteract inertial effects to some extent as can be seen from RDT results. Thus we can say that inertial term has anisotropizing effect and pressure term initially has isotropizing effect on turbulence evolution. In case of 2C2 initial condition both models predict no evolution at all as both the production and rapid pressure terms are found to be zero at all times (Figures not shown).

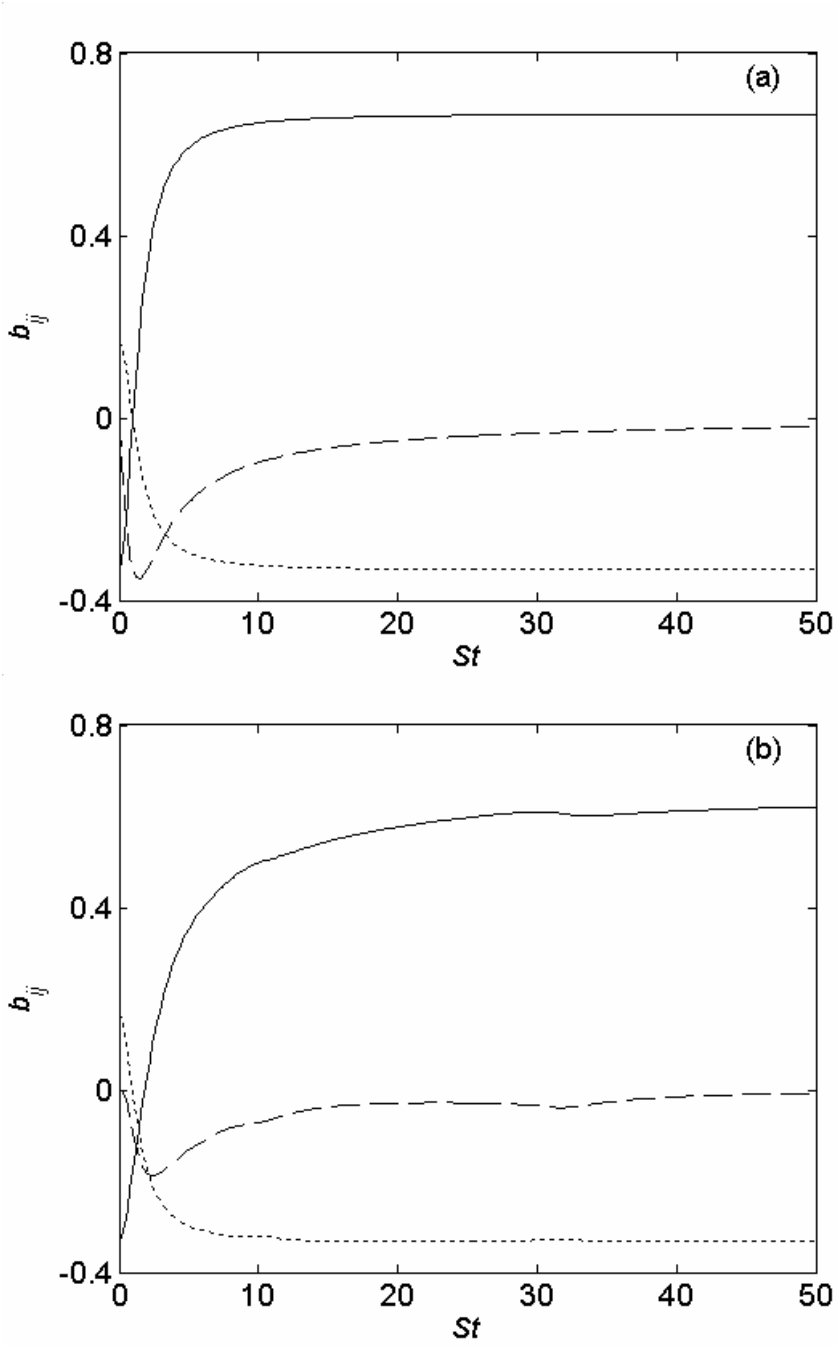

FIG. 10. Evolution of b_{ij}. Mean flow: Case 1. Initial condition: 2C1. (a) RDT–B and (b) RDT. Legend: (—) - $b_{11,}$ (•••) - b_{22}, (– – –) - b_{12}.

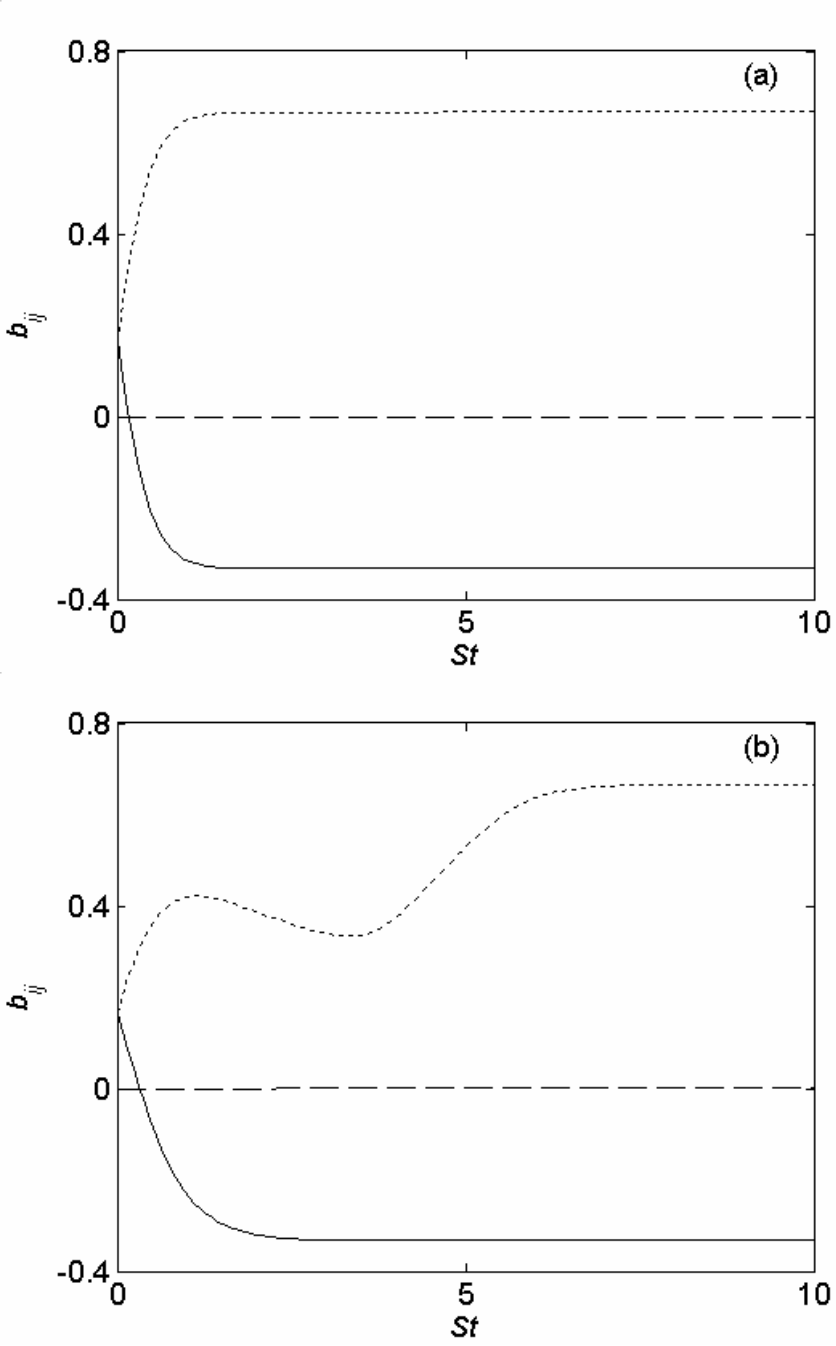

Fig. 11. Evolution of b_{ij}. Mean flow: Case 2. Initial condition: 2C3. (a) RDT-B and (b) RDT. Legend as given in Fig. 9.

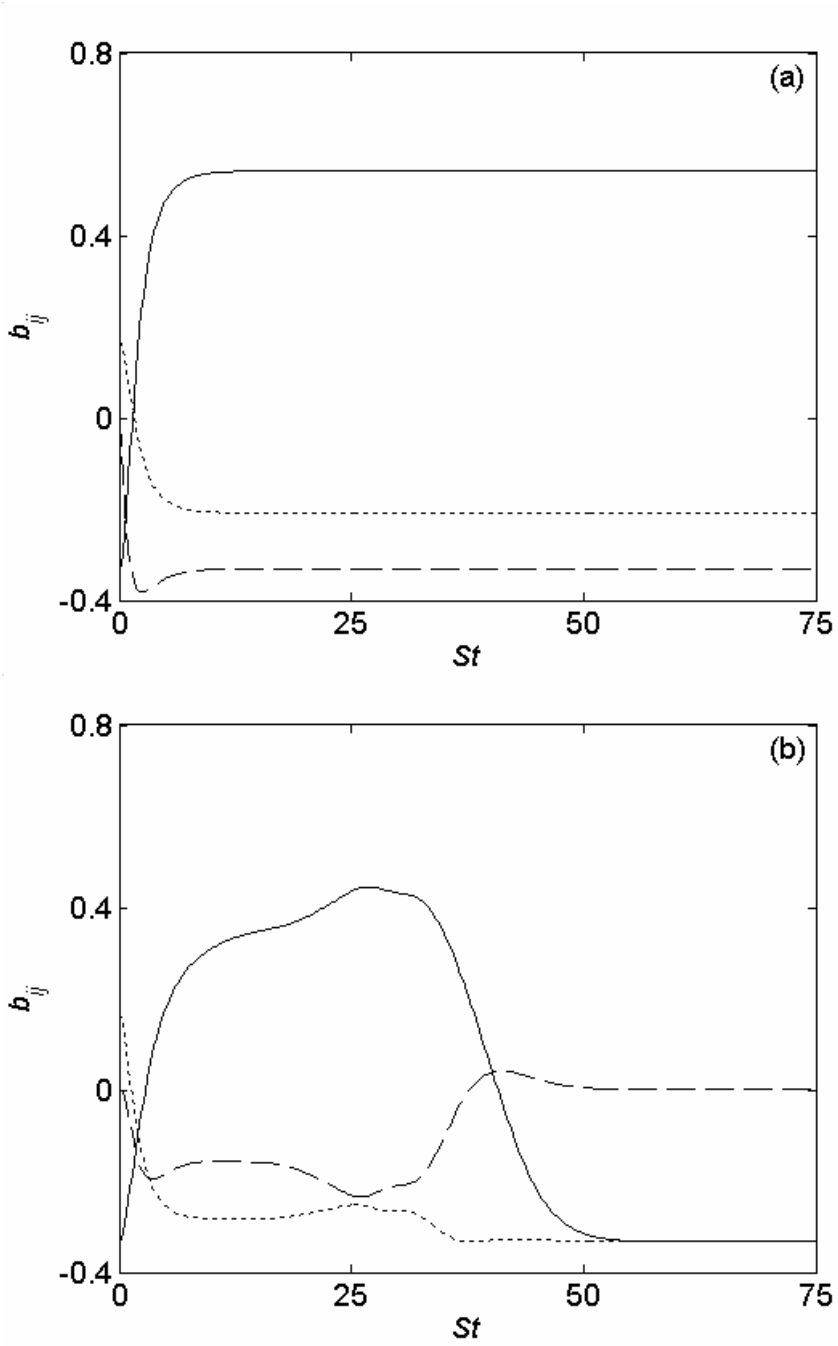

FIG. 12. Evolution of b_{ij}. Mean flow: Case 3. Initial condition: 2C1. (a) RDT-B and (b) RDT. Legend as given in Fig. 8.

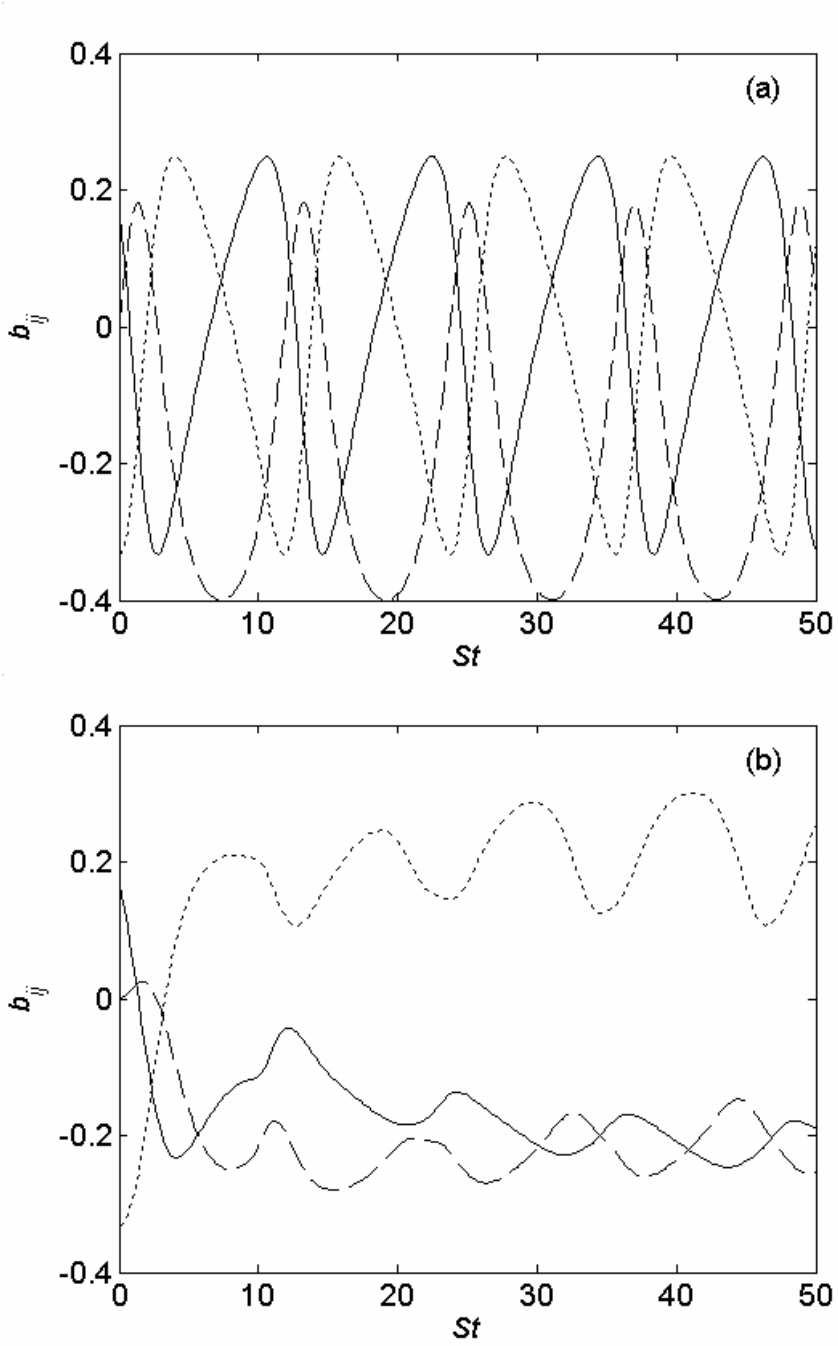

FIG. 13. Evolution of b_{ij}. Mean flow: Case 4. Initial condition: 2C2. (a) RDT-B, (b) RDT. Legend as given in Fig. 8.

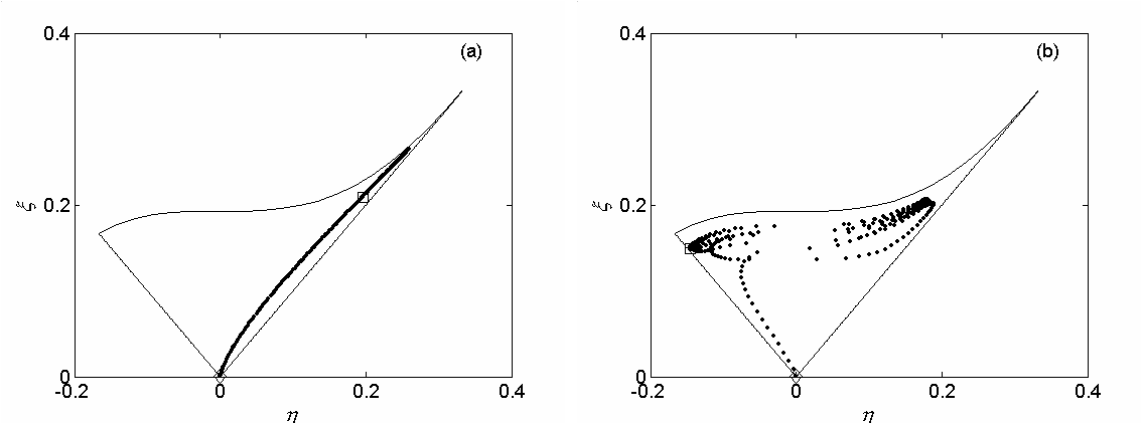

FIG.14. Lumley triangle for mean flow: Case 5. Initial condition: ISO. (a) RDT-B and (b) RDT. Legend: (◊) – starting point and (□) – end point.

Evolution of turbulence subjected to plane strain mean flow is shown in Fig. 11. In this case we find that b_{ij} from both RDT and RDT-B takes considerably less time to reach the asymptotic state compared to the homogeneous shear case. Even though the evolution is different initially, at later times RDT-B and RDT agree perfectly and hence we can say that pressure has no effect at all. For Case 3 – another strain dominated flow – the RDT-B and RDT predictions are widely different (Fig. 12). The asymptotic agreement of b_{ij} that was seen in the earlier cases is not found here. Even though both RDT-B and RDT predict the flow to reach an asymptotic state, the fixed points predicted by RDT-B and RDT are completely different.

The evolution of b_{ij} for a rotation dominated flow (case 4) with 2C2 initial condition is shown in Fig. 13. Both the models predict widely different but oscillating evolution of b_{ij}. The only qualitative difference is that the RDT results are relatively damped

compared to the RDT-B results. This can again be attributed to the isotropizing role of the rapid pressure term. Fig. 14 shows the evolution of anisotropy tensor invariants on a Lumley triangle for Case 5 with isotropic initial condition. The trajectories predicted by RDT and RDT-B are distinctly different. It is noted that the tendency to move to 1C limit – which is seen in all strain-dominated cases – is not observed here.

2.3.4 RDT-BC results

The results with incompressibility artificially enforced in the RDT-B model calculations are now presented. It is found that RDT-BC results are identical to RDT results in all our computations. The evolution of b_{ij} subjected to Homogeneous Shear mean deformation is shown in Fig. 15. Both RDT-BC and RDT (Fig. 10b) predict exactly similar evolutions at all the times. Now we look at the third strain dominated flow where our RDT-B and RDT results disagreed completely. In this case too we have total agreement between RDT-BC and RDT predictions (Fig. 16 and Fig. 12b). In the two rotation-dominated flows considered we again observed a perfect agreement between RDT-BC and RDT results. Fig. 17 shows the evolution of anisotropy tensor for Case 4 with 2C2 initial condition. Therefore we have numerically shown that the correction prescribed by us will always result in the recovery of RDT results irrespective of mean flow and initial conditions. Thus we conclude that the role of rapid pressure term is to merely impose incompressibility constraint on turbulence evolution in the manner given by Eqn. (2.28).

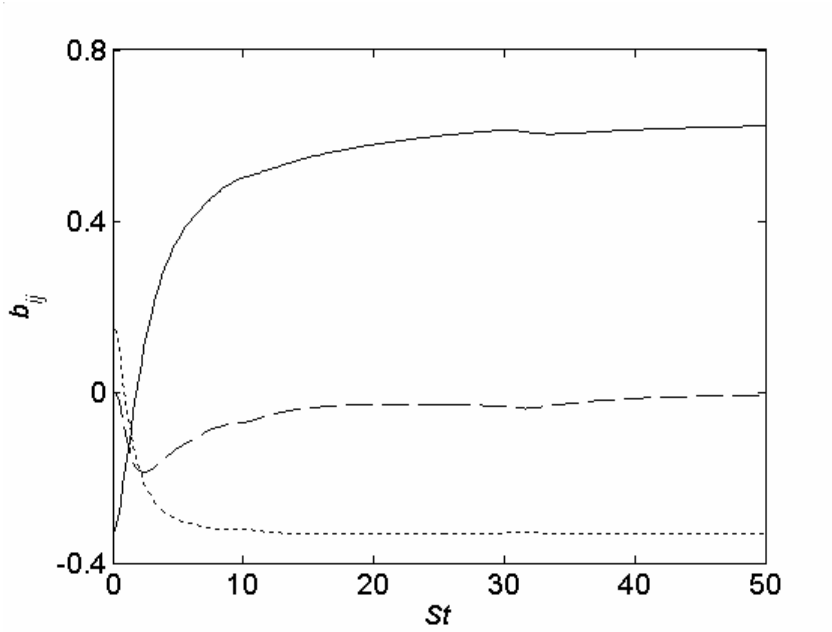

FIG. 15. Evolution of b_{ij} from RDT-BC. Mean flow: case 1. Initial Condition: 2C1. Legend as given in Fig. 8.

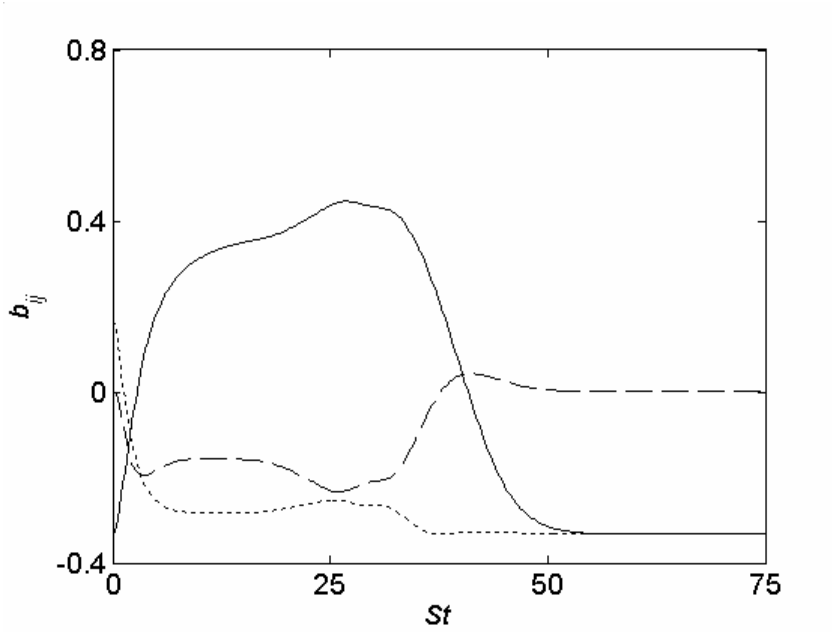

FIG. 16. Evolution of b_{ij} from RDT-BC. Mean flow: Case 3. Initial condition: 2C1. Legend as given in Fig. 6.

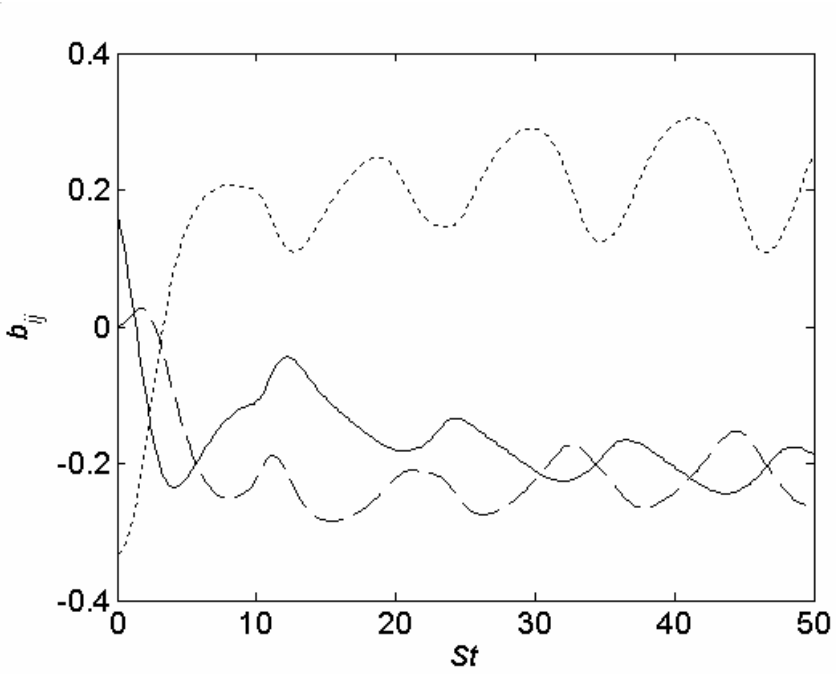

FIG. 17. Evolution of b_{ij} from RDT-BC. Mean flow: Case 4. Initial condition: 2C2. Legend as given in Fig. 6.

CHAPTER III

VELOCITY GRADIENT DYNAMICS OF BURGERS TURBULENCE

We now turn our attention to non-linear aspects of inertial and pressure effects. Non-linearity introduces complications such as invalidity of superimposition and convolution integration that render solution in Fourier space expensive. A more convenient approach is to investigate simplified velocity gradient evolution equations derived from either Navier-Stokes or Burgers equations in physical space. The idea is to derive a simple autonomous set of ordinary differential equations for velocity gradient evolution following a fixed particle. This line of inquiry was first introduced by Vieillefosse [5] and the resulting system of equations was given the name restricted Euler equations.

3.1 Governing equations

In this section, we first derive the 3D Burgers equation for velocity gradient tensor. The evolution equations for strain-rate tensor and rotation tensor are then obtained. Finally we present the restricted Euler equation.

3.1.1. Burgers equations

The inviscid 3D Burgers equation, given by

$$\frac{\partial u_i}{\partial t} + u_k \frac{\partial u_i}{\partial x_k} = 0 \tag{3.1}$$

is differentiated with respect to x_j leading to

$$\frac{\partial A_{ij}}{\partial t} + u_k \frac{\partial A_{ij}}{\partial x_k} + A_{ik} A_{kj} = 0 \quad \text{or} \quad \frac{dA_{ij}}{dt} + A_{ik} A_{kj} = 0 . \tag{3.2}$$

where A_{ij} is the velocity gradient tensor, $A_{ij} = \frac{\partial u_i}{\partial x_j}$ and $\frac{d}{dt}$ represents Lagrangian derivative. The incompressibility condition is not satisfied as Burgers equation does not include pressure term. As viscous effects are also neglected, the evolution equation for A_{ij} may diverge in finite time and therefore these equations are not suitable for numerical computations. In order to overcome this problem, a normalized velocity gradient tensor (b_{ij}) is defined [7]

$$b_{ij} = \frac{A_{ij}}{\sqrt{\varepsilon}} \quad \text{where } \varepsilon = A_{mn} A_{mn} . \tag{3.3}$$

The b_{ij} tensor contains all the geometric information of the velocity gradient tensor (A_{ij}) and is better suited for numerical computations. The evolution equation of b_{ij} can now be obtained from Eq. (3.2)

$$\frac{\partial b_{ij}}{\partial t} = -\sqrt{\varepsilon}\left(b_{ik} b_{kj} - b_{ij} b_{mn} b_{mk} b_{kn}\right). \tag{3.4}$$

This equation still contains $\sqrt{\varepsilon}$ which may diverge in finite time. Since we are interested in the asymptotic behavior of the velocity gradient tensor such a divergence is not desirable. Therefore the evolution of b_{ij} is studied in normalized time

$$\partial t' = \sqrt{\varepsilon}\,\partial t . \tag{3.5}$$

Eq. (3.4) can now be rewritten as

$$\frac{\partial b_{ij}}{\partial t'} = -\left(b_{ik}b_{kj} - b_{ij}b_{mn}b_{mk}b_{kn}\right). \tag{3.6}$$

This is a simple first-order differential equation that can be solved numerically for b_{ij} given the initial condition. As we are interested in the behavior of strain-rate tensor and vorticity, the velocity gradient tensor is decomposed into its symmetric part (strain-rate tensor, s_{ij}) and the anti-symmetric part (rotation tensor, w_{ij}). Eq. (3.6) can now be used to obtain separate evolution equations for s_{ij} and w_{ij}

$$\frac{\partial s_{ij}}{\partial t'} = s_{ij}(b_{mn}b_{mk}b_{kn}) - s_{ik}s_{kj} - w_{ik}w_{kj}\,; \tag{3.7}$$

$$\frac{\partial w_{ij}}{\partial t'} = w_{ij}(b_{mn}b_{mk}b_{kn}) - s_{ik}w_{kj} - w_{ik}s_{kj}\,. \tag{3.8}$$

Eq. (3.7) and (3.8) are used to obtain analytical asymptotic solutions from fixed point analysis.

3.1.2 Restricted Euler equations

The Euler equations in terms of velocity gradients for inviscid incompressible can be written as [6]

$$\frac{dA_{ij}}{dt} + A_{ik}A_{kj} - A_{mk}A_{km}\frac{\delta_{ij}}{3} = H_{ij} \tag{3.9}$$

where $H_{ij} = -\left(\frac{\partial^2 p}{\partial x_i \partial x_j} - \frac{\partial^2 p}{\partial x_k \partial x_k}\frac{\delta_{ij}}{3}\right)$.

In this work, we follow the precedent of Vieillefosse [5], Cantwell [6] and Girimaji *et al* [7] and neglect the pressure Hessian ($H_{ij} = 0$) restricting ourselves to isotropic turbulence. An analysis similar to that used for Burgers equations leads to

$$\frac{\partial b_{ij}}{\partial t'} = -\left(b_{ik}b_{kj} - \frac{1}{3}(b_{mk}b_{kn})\delta_{ij} - b_{ij}b_{mn}b_{mk}b_{kn} \right) \tag{3.10}$$

and the corresponding evolution equations for s_{ij} and w_{ij} are given by

$$\frac{\partial s_{ij}}{\partial t'} = s_{ij}(b_{mn}b_{mk}b_{kn}) + \frac{1}{3}(b_{mk}b_{kn})\delta_{ij} - s_{ik}s_{kj} - w_{ik}w_{kj}\,; \tag{3.11}$$

$$\frac{\partial w_{ij}}{\partial t'} = w_{ij}(b_{mn}b_{mk}b_{kn}) - s_{ik}w_{kj} - w_{ik}s_{kj}\,. \tag{3.12}$$

The velocity gradient dynamics are studied in terms of its invariants as proposed by Cantwell [6]. The various velocity gradient invariants are:

$$\begin{aligned} &P(t') = -b_{ii}\,; \qquad Q(t') = -\frac{1}{2}b_{im}b_{mi}\,; \\ &\text{and } R(t') = -\frac{1}{3}b_{im}b_{mk}b_{ki}\,. \end{aligned} \tag{3.13}$$

Each of these invariants has a specific physical significance in the context of turbulent flows. $P(t')$ is the dilatation (with negative sign) of the velocity field. Negative $P(t')$ (positive dilatation) implies that the fluid particle is expanding and positive $P(t')$ means that the particle is contracting. The fact that incompressibility is satisfied in case of the restricted Euler equations means that $P(t') = 0$ whereas it is not necessarily satisfied with the Burgers equations. $Q(t')$ represents the difference between the magnitude of strain and vorticity. If $Q(t')$ is positive, then the magnitude of rotation exceeds that of

strain and vice versa. $R(t')$ is an indicator of the energy cascade rate or gradient steepening. Positive $R(t')$ indicates forward energy cascade from large scales to small scales whereas negative $R(t')$ implies inverse energy cascading.

In our work, numerical computations are performed to calculate the velocity gradient tensor in the asymptotic limit and its invariant (Q *Vs* R) behavior is examined.

3.2 Results and discussion

The analytical asymptotic solutions are obtained by fixed point analysis of the governing equations. Fixed point analysis yields all the possible solutions some of which may not be stable. Since the governing equations are quite complicated a formal stability analysis is not feasible. Hence numerical computations are performed to identify the stable solutions. First, the analytical and numerical results from restricted Euler equations are presented. The properties of velocity gradient tensor, which have already been addressed in previous works [5, 6] are discussed briefly. Next, the stable solutions of Burgers equations are identified and are further examined to investigate the properties of velocity gradient tensor in the asymptotic limit and the applicability of these solutions to compressible turbulence. The results from Burgers equations are then compared with the restricted Euler results to distinguish the effect of pressure and inertial terms. The difference between Burgers and restricted Euler solutions may also reflect the difference between cascade physics in incompressible and compressible flows.

3.2.1 Asymptotic solutions to restricted Euler equation

The fixed point equations can be obtained from Eq. (3.11) and (3.12) by setting the left-hand side to zero:

$$s_{ij}(b_{mn}b_{mk}b_{kn}) + \frac{1}{3}(b_{mk}b_{kn})\delta_{ij} - s_{ik}s_{kj} - w_{ik}w_{kj} = 0\,; \tag{3.14}$$

$$w_{ij}(b_{mn}b_{mk}b_{kn}) - s_{ik}w_{kj} - w_{ik}s_{kj} = 0$$

The analytical solutions to the fixed point equations are:

$$s_{ii} = \frac{s_{ik}s_{kj} - w_{ik}w_{kj} - \frac{1}{3}(b_{mk}b_{kn})\delta_{ij}}{b_{mn}b_{mk}b_{kn}}; \quad \text{for } i,j = 1,2,3. \tag{3.15}$$

$$w_{ij} = \frac{w_{ik}s_{kj} - w_{ik}s_{kj}}{b_{mn}b_{mk}b_{kn}}.$$

These solutions need further investigation. Without loss of generality, we can assume that the coordinate axes of reference are aligned with the principle strain-rate tensor in the asymptotic limit. Hence the s_{ij} and w_{ij} tensors are of the form

$$s_{ij} = \begin{vmatrix} s_{11} & 0 & 0 \\ 0 & s_{22} & 0 \\ 0 & 0 & s_{33} \end{vmatrix} \quad \text{and} \quad w_{ij} = \begin{vmatrix} 0 & w_{12} & w_{13} \\ -w_{12} & 0 & w_{23} \\ -w_{13} & -w_{23} & 0 \end{vmatrix} \tag{3.16}$$

In other words, (s_{11}, s_{22}, s_{33}) are the eigenvalues of the strain-rate tensor. We also arrange the solutions such that $s_{11} \le s_{22} \le s_{33}$. We can then simplify Eq. (3.15) to a set of 6 equations with 6 unknowns. These equations are additionally subject to the constraint that the norm of b_{ij} tensor be equal to unity by definition:

$$s_{11}^2 + s_{22}^2 + s_{33}^2 + 2(w_{12}^2 + w_{13}^2 + w_{23}^2) = 1 \tag{3.17}$$

The incompressibility condition is automatically satisfied by the fixed point solution. These nonlinear set of equations are solved analytically in MATHCAD. The fixed points for this system of nonlinear equations are given by:

Set 1: (3.18)

$(s_{11}, s_{22}, s_{33}) = (0,0,0)$ and $w_{12} = \pm\frac{1}{\sqrt{6}}$, $w_{13} = \pm\frac{1}{\sqrt{6}}$, $w_{23} = \pm\frac{1}{\sqrt{6}}$ (all eight different possible combinations)

Set 2:

$$(s_{11}, s_{22}, s_{33}, w_{12}, w_{13}, w_{23}) =$$

$$\left(\frac{1}{3}\frac{(w_{13}^2 - 1)}{\sqrt{-\frac{2}{3}\cdot w_{13}^2 + \frac{5}{12} + y}}, -\frac{1}{3}\frac{(-w_{13}^2 + \frac{1}{4} + 3y)}{\sqrt{-\frac{2}{3}\cdot w_{13}^2 + \frac{5}{12} + y}}, \sqrt{-\frac{2}{3}\cdot w_{13}^2 + \frac{5}{12} + y}, 0, w_{13}, 0 \right);$$

Set 3:

$$(s_{11}, s_{22}, s_{33}, w_{12}, w_{13}, w_{23}) =$$

$$\left(\frac{1}{3}\frac{(w_{13}^2 - 1)}{\sqrt{-\frac{2}{3}\cdot w_{13}^2 + \frac{5}{12} - y}}, -\frac{1}{3}\frac{(-w_{13}^2 + \frac{1}{4} - 3y)}{\sqrt{-\frac{2}{3}\cdot w_{13}^2 + \frac{5}{12} - y}}, \sqrt{-\frac{2}{3}\cdot w_{13}^2 + \frac{5}{12} - y}, 0, w_{13}, 0 \right);$$

where $y = \frac{1}{12}\cdot\sqrt{48\cdot w_{13}^4 - 48\cdot w_{13}^2 + 9}$.

Set 1 has no free parameters. Set 2 and Set 3 represent a family of fixed points parameterized by w_{13}. To identify the stable solutions, Equation (3.10) is solved numerically using the fourth order Runge-Kutta method. We randomly generate 500 different initial velocity gradient tensors ($b_{ij}(t' = 0)$) and compute the corresponding velocity gradient tensors in the asymptotic limit. These results are studied in terms of the

invariants of b_{ij} tensor (Q *Vs* R). In case of restricted Euler equations, an analytical relation can be obtained that relates the invariants (Q, R) [6]

$$R = \pm(-\frac{4}{27}Q^3)^{1/2}. \tag{3.19}$$

Fig. 18 shows the invariant Q *vs* R plot from numerical computations of restricted Euler equations. Each point corresponds to the asymptotic state reached from a random initial condition. Expectedly, all the points lie on the trajectory prescribed by Eq. (3.19). It is found that all the points on the figure correspond to Set 3 of the fixed point sets given in

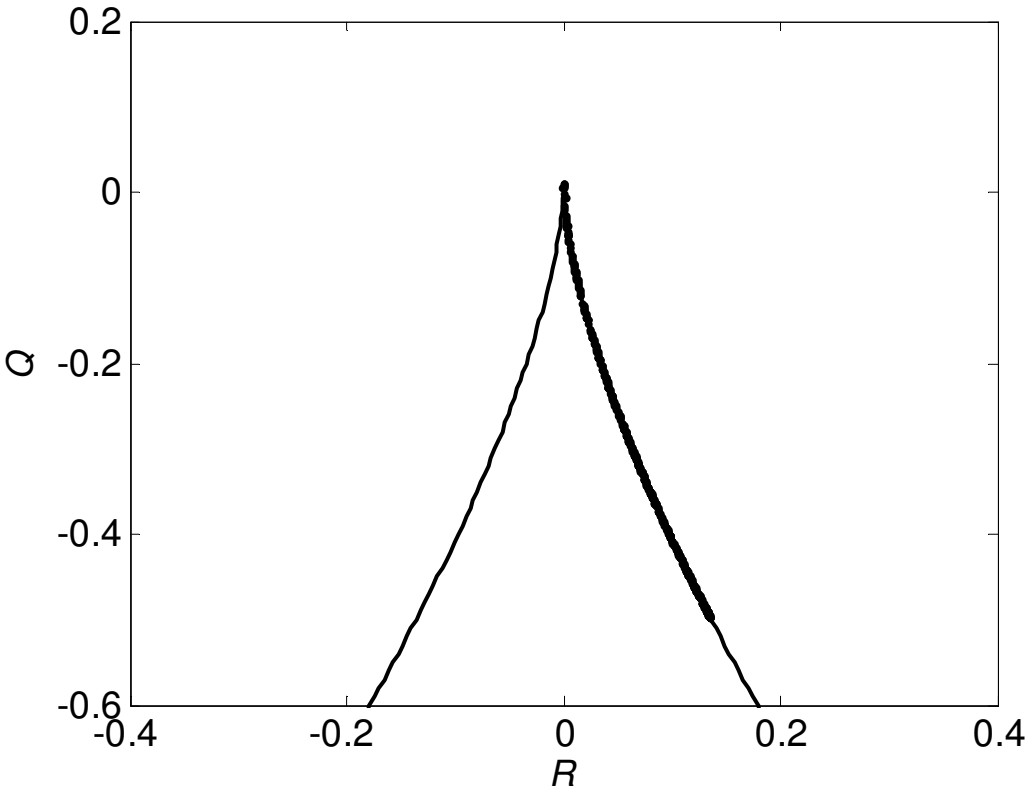

FIG. 18. The invariant plot from computations of restricted Euler equation.
Legend: (—) – Eq. (3.19). (•) – restricted Euler computations.

Eq. (3.18). Therefore, the stable fixed point is a family of solutions with one free parameter (w_{13}).

We investigate further into the properties of the stable solution – Set 3. Figure 19 show the PDF of principal strain-rates from numerical computations. We can clearly see that the intermediate strain-rate s_{22} is positive and has the smallest magnitude compared to the other two strain-rates. The vorticity vector ($\vec{\omega}$) is related to the rotation tensor (w_{ij}) by the Levi-Civita tensor (e_{ijk})

$$\omega_k = \frac{1}{2} e_{ijk} w_{ij} . \tag{3.20}$$

Using this relation, the vorticity vector corresponding to the stable fixed point is calculated

$$(\omega_1, \omega_2, \omega_3) = (0, -w_{13}, 0) . \tag{3.21}$$

It can be seen that the vorticity vector has only one component (ω_2) and it is indeed aligned with the intermediate strain-rate (s_{22}). Energy cascade can be studied in terms of the rate of change of magnitude of the velocity gradient tensor (ε). A positive rate of change of ε is an indication that energy is being transferred from large scales to small scales. The evolution of ε can be obtained using Eq. (3.9)

$$\frac{d\varepsilon}{dt} = -2 A_{mk} A_{kn} A_{mn} . \tag{3.22}$$

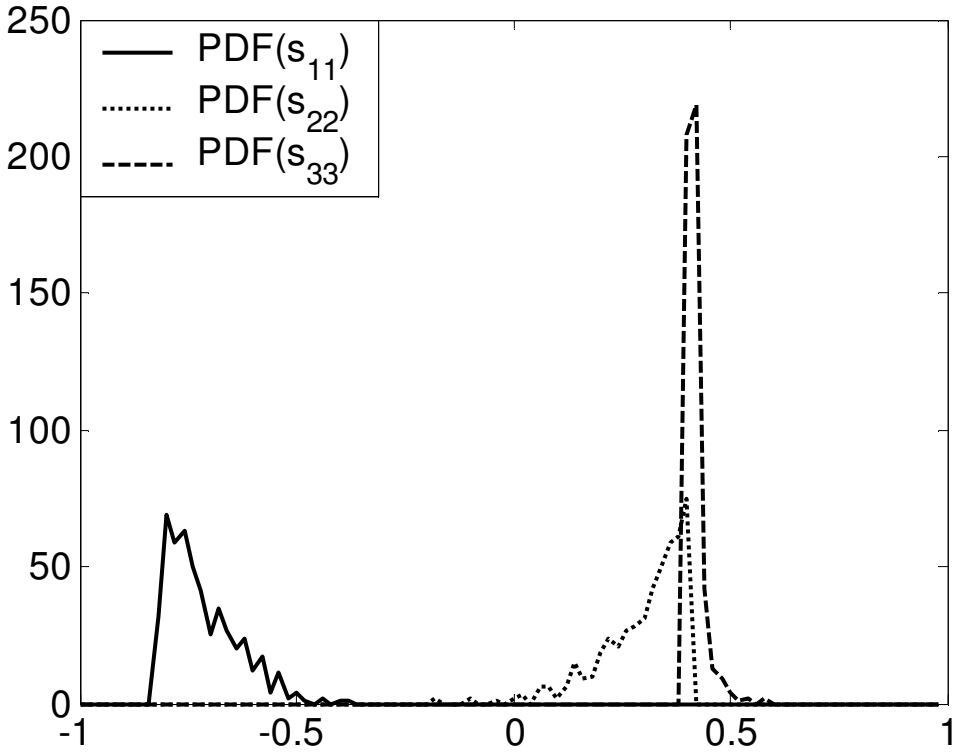

FIG. 19. The PDF of asymptotic principal strain-rates from computations of restricted Euler equations.

In the asymptotic limit, decomposing A_{ij} into its symmetric and anti-symmetric parts and using the form defined by Eq. (3.16) for s_{ij} and w_{ij}, the right-hand side of Eq. (3.22) can be rewritten as

$$\frac{d\varepsilon}{dt'} = -2\varepsilon(s_{11}(s_{11}^2 + w_{12}^2 + w_{13}^2) + s_{22}(s_{22}^2 + w_{12}^2 + w_{23}^2) + s_{33}(s_{33}^2 + w_{13}^2 + w_{23}^2)) . \tag{3.23}$$

Upon substituting the stable solution and simplifying, we have

$$\frac{d\varepsilon}{dt'} = 2\varepsilon(s_{22}) . \tag{3.24}$$

Since it is already proved that s_{22} is non-negative, the right-hand side of Eq. (3.24) is non negative. This is a clear evidence of forward energy cascade in incompressible turbulent flows. In Fig. 18, we note that $R(t')$ is positive in all the numerical computations which further confirms the forward energy cascade. In summary, we have been able to (i) reproduce the trends and results obtained earlier in [5] and [6] and, (ii) explain energy cascade using the analytical results.

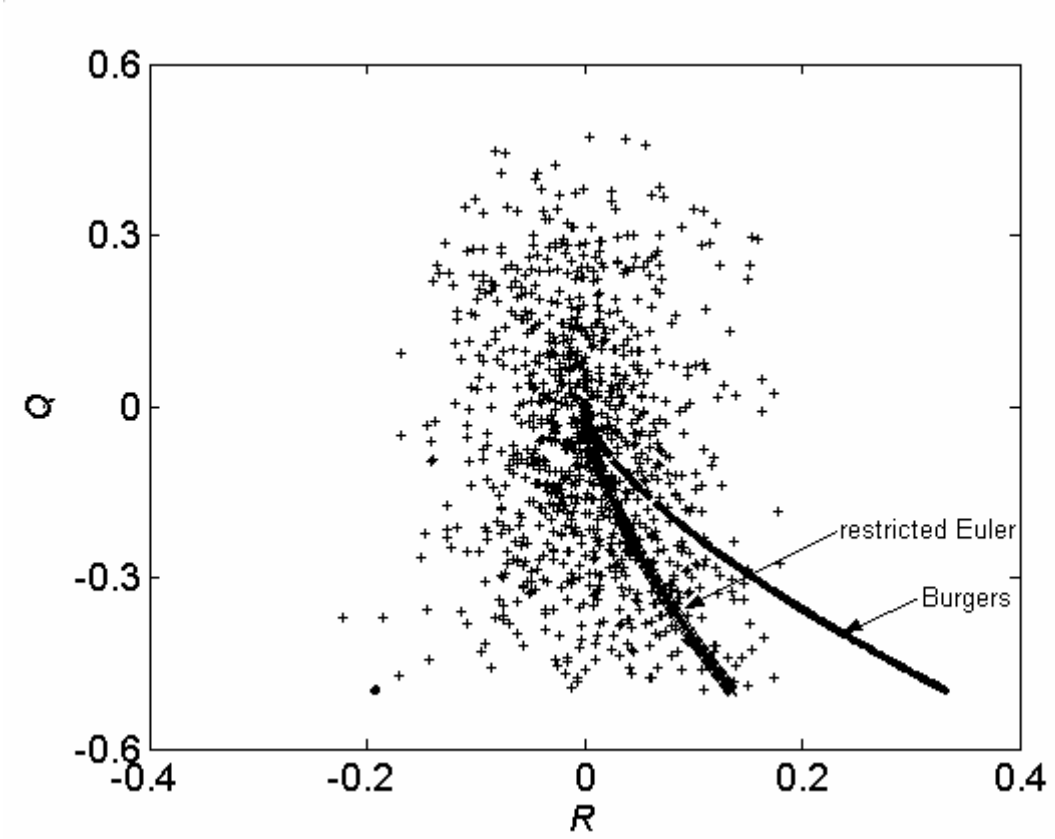

FIG. 20. DNS results of decaying isotropic turbulence. Legend: (+) – DNS result.

We also compare the numerical computations of restricted Euler equations with Direct Numerical Simulation (DNS) of decaying isotropic and homogeneous anisotropic velocity fields. The decaying isotropic DNS data is obtained from [12] and the homogeneous anisotropic DNS data is obtained from [13]. Figures 20 and 21 show the DNS results of decaying isotropic and decaying homogeneous anisotropic velocity fields respectively. It is to be noted that the invariants in DNS scatter plots are calculated from the normalized velocity gradients.

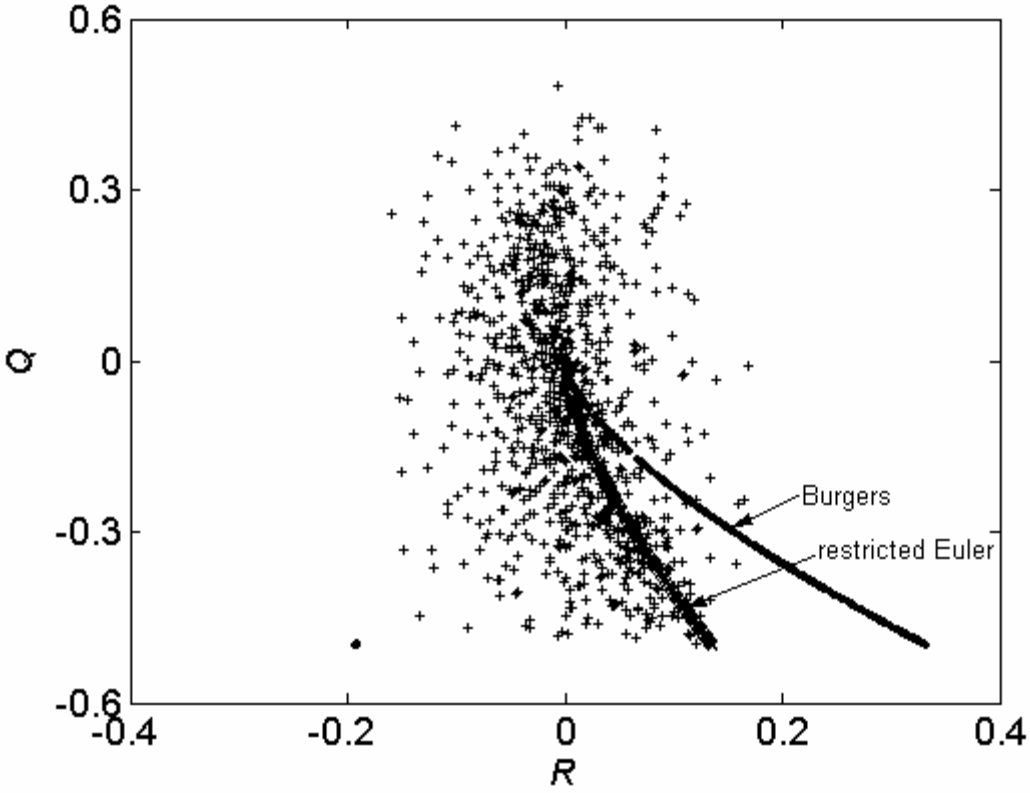

FIG. 21. DNS results of decaying homogeneous anisotropic turbulence. (+) – DNS result.

3.2.2 Asymptotic solutions to Burgers equation

The fixed point equations are obtained from Eq. (3.7) and (3.8) by setting the left-hand side to zero:

$$s_{ij}(b_{mn}b_{mk}b_{kn}) - s_{ik}s_{kj} - w_{ik}w_{kj} = 0; \tag{3.25}$$

$$w_{ij}(b_{mn}b_{mk}b_{kn}) - s_{ik}w_{kj} - w_{ik}s_{kj} = 0$$

The fixed points are given by:

$$s_{ij} = \frac{s_{ik}s_{kj} - w_{ik}w_{kj}}{b_{mn}b_{mk}b_{kn}} \quad \text{and} \quad w_{ij} = \frac{w_{ik}s_{kj} - w_{ik}s_{kj}}{b_{mn}b_{mk}b_{kn}}. \text{ for } i,j = 1,2,3. \tag{3.26}$$

Again, these equations are subject to the constraint that the norm of b_{ij} tensor equals unity (Eq. (3.17)). Solving these equations for principal rates of strain and rotations tensor we get four sets of asymptotic solutions:

Set 1: $(s_{11}, s_{22}, s_{33}, w_{12}, w_{13}, w_{23}) = (-\frac{1}{\sqrt{3}}, -\frac{1}{\sqrt{3}}, -\frac{1}{\sqrt{3}}, 0, 0, 0)$, (3.27)

Set 2: $(s_{11}, s_{22}, s_{33}, w_{12}, w_{13}, w_{23}) = (\frac{1}{\sqrt{3}}, \frac{1}{\sqrt{3}}, \frac{1}{\sqrt{3}}, 0, 0, 0)$,

Set 3: $(s_{11}, s_{22}, s_{33}, w_{12}, w_{13}, w_{23}) = (s_{33} - 1, 0, s_{33}, 0, \pm\sqrt{s_{33} - s_{33}^2}, 0)$,

Set 4: $(s_{11}, s_{22}, s_{33}, w_{12}, w_{13}, w_{23}) = (-z, -z + s_{33}, s_{33}, 0, \pm\sqrt{s_{33} \cdot z}, 0)$,

where $z = \frac{1}{2}\sqrt{2 - 4s_{33}^2}$.

Set 3 and Set 4 are characterized by a single free parameter s_{33}. These solutions constitute the entire possible fixed point solution set – both stable and unstable solutions. Note that incompressibility condition is not satisfied by these solutions ($\sum s_{ii} \neq 0$).

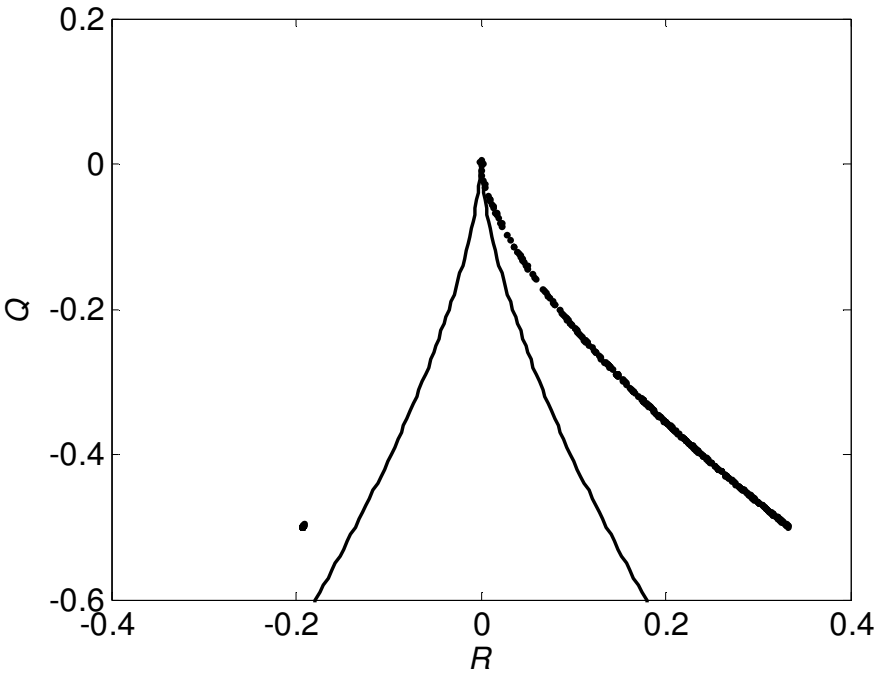

FIG. 22. The invariant plot from computations of Burgers equations. Legend: (—) – Eq. (8.6). (•) – from Burgers computations.

Numerical computations of Equation (3.6) are performed using the fourth order Runge-Kutta method. In this case too, 500 different randomly generated initial velocity gradient fields ($b_{ij}(t'=0)$) are used. Fig. 22 shows the (Q *vs* R) plot for Burgers equations. From the numerical results, we find that fixed point Set 2, 3 are stable. Set 2 corresponds to the single fixed point as seen in the third quadrant of Fig. 22 and Set 3 corresponds to the

continuous branch in the fourth quadrant. It is observed from the numerical results that nearly 30% of points correspond to Set 2 and the rest correspond to Set 3 of the two stable sets. Hence we can say that Set 2 is the minor attractor and Set 3 is the major attractor. It is expected these two sets of fixed points constitute the solutions of high Mach number compressible turbulence.

Let us now examine the properties of the stable solution sets in detail. In case of the major attractor Set 3, the intermediate principal strain-rate is zero as opposed to being positive as observed in case of restricted Euler solutions. The vorticity vectors corresponding to the stable fixed point sets 2, 3 are calculated

Set 2 - $(\omega_1, \omega_2, \omega_3) = (0,0,0)$, (3.28)

Set 3 - $(\omega_1, \omega_2, \omega_3) = (0, \mp\sqrt{s_{33} - s_{33}^2}, 0)$.

It can be seen that in case of Set 3, ω_2 is the only non-zero component. Hence the vorticity vector is aligned with the intermediate strain-rate (s_{22}) which is zero. This could imply that vortex stretching is inhibited in compressible turbulence. In case of Set 2, there is no vorticity at all. Energy cascading is studied further in terms of rate of change of ε as done earlier with restricted Euler equations. The equation for ε is incidentally same for both restricted Euler and Burgers equations. Hence, using Eq. (3.22), the evolution equations for ε corresponding to each stable set are:

Set 2: $\frac{d\varepsilon}{dt'} = -\frac{\varepsilon}{\sqrt{3}}$, (3.29)

Set 3: $\frac{d\varepsilon}{dt'} = \varepsilon(1-2s_{33})$.

The right-hand side, in case of Set 3, is always positive as the numerical computations indicate that all the points belonging to the fixed point Set 3 are such that $s_{33} \leq 0.5$. Hence, in this case we have positive growth of velocity gradients which implies forward energy cascade as expected. With Set 2, the right-hand side is negative indicating that energy is transferred from small scales to large scales i.e. inverse energy cascading. This is consistent with the numerical computations (fig. 22) – $R(t')$ is negative for Set 2 indicating inverse energy cascade whereas it is positive for Set 3 implying forward cascading. We also note that the first invariant $P(t')$ is negative for Set 2 implying that the particles are expanding and it is positive for Set 3 indicating that the particles are contracting. In effect, the particles that are expanding experience inverse energy cascade and the particles that are contracting undergo forward energy cascade. This kind of bimodal behavior – simultaneous direct and inverse energy cascade – has been observed in earlier studies of compressible turbulence and magnetohydrodynamic turbulence [14, 15, 16, 17].

3.2.3 Effect of pressure

The difference in the numerical results of Burgers and restricted Euler equations can be seen as the effect of pressure. In Fig 22, we find that the invariant R corresponding to Set 3 is higher in magnitude compared to that in restricted Euler computations (Fig.18). This

indicates faster energy cascade in Burgers turbulence. Whereas, the invariant R corresponding to Set 2 is negative, further confirming the inverse energy cascade which was noted earlier with analytical solutions. Comparing the Burgers and restricted Euler results, we can say that pressure causes Set 2, 3 to collapse onto the restricted Euler results. Specifically, the effect of pressure is to moderate the energy cascade rate of Set 3 and negate the inverse cascade effect in case of Set 2.

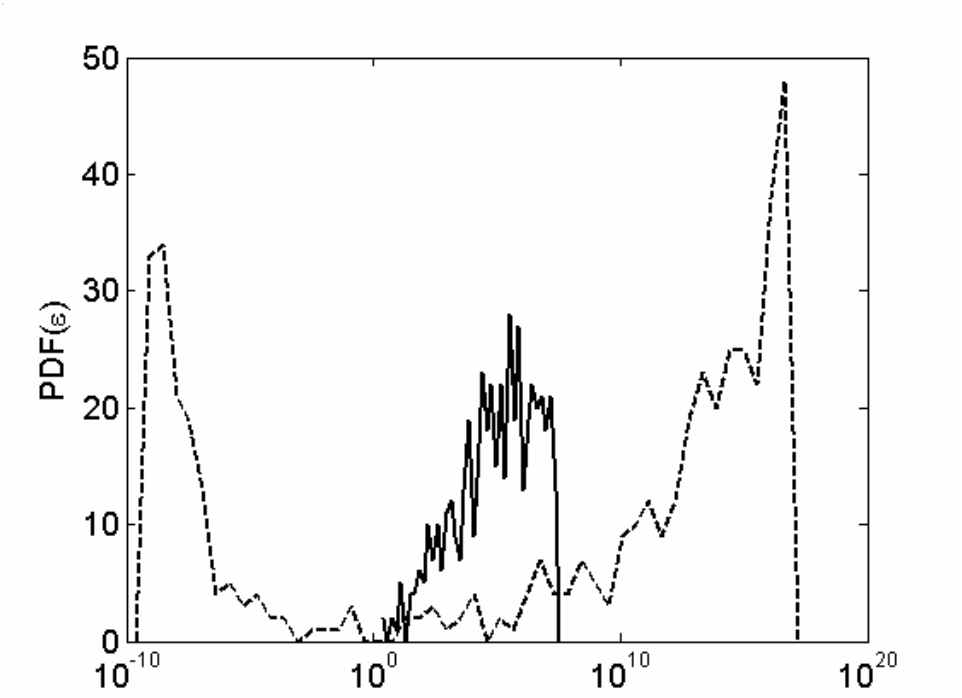

FIG. 23. The PDF of magnitude of velocity gradient tensor (ε) in the asymptotic limit. Legend: Solid line - restricted Euler results, dashed line – Burgers results.

We also obtain the actual magnitude of velocity gradients (ε) numerically in the asymptotic limit to better demonstrate the energy cascade. Large magnitudes of ε implies gradient steepening i.e. forward energy cascade and very low magnitudes imply

gradient smoothening or inverse energy cascading. Fig. 23 shows the PDF of asymptotic ε's from both Burgers and restricted Euler computations. In case of Burgers results, we have two distinctly concentrated regions – one at very high magnitudes and the other at low magnitudes. From the numerical computations, it is found that all the low magnitude ε's correspond to Set 2 whereas the high magnitude ε's correspond to Set 3. The restricted Euler ε's are concentrated in the intermediate range. This further confirms that, in Burgers turbulence: (i) in regions governed by Set 3 where particles are contracting, energy cascade is faster than in incompressible turbulence (ii) in regions dominated by Set 2 behavior i.e. expanding particles, there is inverse energy cascade.

3.2.4 Restricted Burgers equation

A third class of equations that one can possibly consider is the evolution of the anisotropic part of Burgers turbulence velocity gradients. The velocity gradient anisotropy tensor is defined as

$$a_{ij} = A_{ij} - \frac{1}{3} A_{pp} \delta_{ij} . \tag{3.30}$$

where A_{ij} evolves according to Burgers equation. Clearly a_{ij} satisfies the incompressibility requirement. When this correction is applied at every time step during the numerical computations of Burgers equations, the ensuing results (Q *Vs* R) are found to be identical to the restricted Euler results. Thus we say that the role of pressure in

restricted Euler equation is merely to kinematically satisfy the incompressibility constraint.

CHAPTER IV

SUMMARY AND CONCLUSIONS

4.1 Inertial and pressure effects in the rapid distortion limit

Inviscid rapid distortion calculations of Navier Stokes (RDT) and Burgers (RDT-B) are performed for a wide range of mean flows and initial turbulence conditions. Rotation-dominated mean flows are also studied along with strain-dominated mean flows. The linear aspects of the role of pressure can be surmised by contrasting RDT and RDT-B results. The precise role of inertial and pressure terms depends on the type of mean flow and also the initial anisotropy of turbulence. The important conclusions from ours findings are

1. In strain-dominated flows, the role of pressure is to inhibit the kinetic energy growth as large times. Indeed the growth rate is zero in the asymptotic limit. Pressure causes $\langle u_1 u_1 \rangle, \langle u_2 u_2 \rangle$ and $\langle u_1 u_2 \rangle$ to go to zero at long times. Therefore production vanishes in the asymptotic limit resulting in the saturation of kinetic energy. In the absence of pressure $\langle u_1 u_1 \rangle, \langle u_2 u_2 \rangle$ and $\langle u_1 u_2 \rangle$ go to nonzero asymptotic values. Thus production remains nonzero at all times resulting in the continuous growth of kinetic energy.
2. In homogeneous shear flow, $\langle u_2 u_2 \rangle$ and $\langle u_3 u_3 \rangle$ are identically equal to zero and $\langle u_1 u_1 \rangle$ is the only non-zero component (1C1 state) in the asymptotic limit. Pressure

does not have a significant role as inertial effects alone (RDT-B) dictate the evolution of turbulence in a fairly accurate manner when compared with RDT.

3. In rotation-dominated flows, the pressure surprisingly causes the kinetic energy to grow at long times. Without pressure, kinetic energy will simply oscillate near the initial value. Pressure causes $\langle u_1 u_1 \rangle, \langle u_2 u_2 \rangle$ and $\langle u_1 u_2 \rangle$ to evolve in such a way that production remains positive at all times. In the absence of pressure, the inertial effect makes production to oscillate about zero.
4. In strain-dominated flows, the RDT-B results (inertial effects only) for anisotropy tensor evolve such that they move from initial isotropic or 2C anisotropic state towards 1C limit in the Lumley triangle. However none if the Reynolds stress components $\langle u_1 u_1 \rangle, \langle u_2 u_2 \rangle$ or $\langle u_1 u_2 \rangle$ completely vanish. On the contrary, the role of pressure is to move the from 2C anisotropic limit to 1C limit such that $\langle u_1 u_1 \rangle, \langle u_2 u_2 \rangle$ and $\langle u_1 u_2 \rangle$ are identically zero in the asymptotic limit. If the initial condition is isotropic, then there is a tendency to move towards 2C limit initially before eventually going to 1C state.
5. In rotation-dominated flows, the anisotropy is periodic with relatively large amplitude in the absence of pressure. The effect of pressure is to moderate the amplitude of anisotropy oscillations in such a manner that overall production remains positive always.
6. When we impose incompressibility forcibly in the RDT-B model calculations by using a correction term, we are able to recover the RDT results for both strain-

dominated and rotation-dominated flows. This implies that the role of rapid pressure is merely to impose incompressibility on the flow field.

We expect that these findings and an improved understanding of the role of pressure will help development of better models for rapid-pressure strain correlation in future.

4.2 Velocity gradient dynamics of Burgers turbulence

The inviscid 3D burgers equation is used to study the velocity gradient dynamics in turbulence evolution. Analytical asymptotic solutions to Burgers equations as well as restricted Euler equations are obtained by fixed point analysis. Numerical computations are then performed to identify the stable solutions. Comparison of invariants of velocity gradient tensor from Burgers and restricted Euler equations enables better understanding of the inertial and pressure effects on velocity gradient dynamics. The analytical solutions of restricted Euler equations are used to reconfirm some of the earlier findings concerning the geometry of velocity gradient tensor: (i) the intermediate principle strain-rate is positive and smaller in magnitude compared to the other two strain-rates and, (ii) Vorticity is aligned with the intermediate strain-rate. A similar analysis of Burgers asymptotic solutions leads to the following conclusions: (i) vortex stretching is inhibited in Burgers turbulence, (ii) predominantly (about 70%), the particles are contracting and forward energy cascade is observed and it proceeds at a faster rate compared to that in restricted Euler solutions; the role of pressure is to moderate the rate of cascading, and (iii) about 30% of the particles are expanding and they undergo inverse energy cascade.

The bimodality observed in our analytical and numerical computations of burgers turbulence is consistent with some of the earlier studies of compressible turbulence. We present a third class of equations – the restricted Burgers equation – where the evolution equation for anisotropic part of Burgers velocity gradient tensor is obtained. It is found from the numerical computations that the results from the restricted Burgers equation are identical those from the restricted Euler equation. Thus we conclude that the role of pressure in restricted Euler equation is solely to kinematically impose incompressibility constraint on turbulence evolution.

REFERENCES

[1] S. S. Girimaji and Y. Zhou, Phys. Lett. A **202**, 279 (1995).

[2] T. Passot and E. Vázquez-Semadeni, Phys. Rev. E. **58**, 4501 (1998)

[3] J.-P. Bouchaud and M. Mezard, Phys. Fluids. **7**, 1438 (1995)

[4] M. Avellaneda, R. Ryan, and W. E, Phys. Fluids. **7**, 3067 (1995).

[5] P. Vieillefosse, J. Phys. (Paris) **43**, 837 (1982).

[6] B.J. Cantwell, Phys. Fluids A. **4**, 782 (1992)

[7] S.S. Girimaji and C.G. Speziale, Phys. Letters A. **202**, 279 (1995)

[8] E. Jeong and S.S. Girimaji, Theoret. Comput. Fluid Dynamics, **16,** 421 (2003)

[9] S. B. Pope, *Turbulent Flows* (Cambridge University Press, Cambridge, 2000)

[10] S.C. Kassinos, W.C. Reynolds, Annual research briefs, Center for Turbulence Research, NASA Ames/Stanford University, 31(1996).

[11] S.S. Girimaji, E. Jeong, and S.V. Poroseva, Phys. of Fluids. **15**, 3209(2003).

[12] H. Yu, S.S. Girimaji, L. Luo, Phys. Rev. E. **71**, 016708 (2005)

[13] D. Yu, to be published in J. Turbulence.

[14] G.Y. Antar, Phys. Rev. Lett. **91**, 055002 (2003)

[15] M. Chertkov, I. Kolokolov and M. Vergassola, Phys. Rev. Lett. **80**, 512 (1998)

[16] M. Christensson, M. Hindmarsh and A. Bradenburg, Phys. Rev. E. **64,** 056405 (2001)

[17] M.A. Rutgers, Phys. Rev. Lett. **81**, 2244(1998)

VITA

Ravi Kiran Bikkani received his Bachelor of Technology degree in mechanical engineering from the Indian Institute of Technology Madras in 2003. He joined Texas A&M University in September 2003 and graduated with a Master of Science degree in aerospace engineering in August 2005. His areas of interest include computational fluid dynamics and turbulence modeling. He can be contacted through Dr. Sharath S. Girimaji at the Aerospace Engineering Department at Texas A&M University, College Station, TX 77843-3141.